A VARIATIONAL APPROACH TO STATIONARY AND ROTATING BOSE-EINSTEIN CONDENSATES

A THESIS

SUBMITTED TO THE DEPARTMENT OF PHYSICS

AND THE INSTITUTE OF ENGINEERING AND SCIENCE

OF BILKENT UNIVERSITY

IN PARTIAL FULFILLMENT OF THE REQUIREMENTS

FOR THE DEGREE OF

MASTER OF SCIENCE

By

Murat Keçeli

July, 2006

I certify that I have read this thesis and that in my opinion it is fully adequate, in scope and in quality, as a thesis for the degree of Master of Science.

Assist. Prof. M. Özgür Oktel (Supervisor)

I certify that I have read this thesis and that in my opinion it is fully adequate, in scope and in quality, as a thesis for the degree of Master of Science.

Prof. Bilal Tanatar

I certify that I have read this thesis and that in my opinion it is fully adequate, in scope and in quality, as a thesis for the degree of Master of Science.

Assoc. Prof. Azer Kerimov

Approved for the Institute of Engineering and Science:

Prof. Mehmet B. Baray
Director of the Institute of Engineering and Science

ABSTRACT

A VARIATIONAL APPROACH TO STATIONARY AND ROTATING BOSE-EINSTEIN CONDENSATES

Murat Keçeli
M.S. in Physics
Supervisor: Assist. Prof. M. Özgür Oktel
July, 2006

After the experimental demonstration of Bose-Einstein condensation (BEC) in alkali gases [6, 7, 18], the number of theoretical and experimental papers on ultracold atomic physics increased enormously [48]. BEC experiments provide a way to manipulate quantum many-body systems, and measure their properties precisely. Although the theory of BEC is simpler compared to other many-body systems due to strong correlation, a fully analytical treatment is generally not possible. Therefore, variational methods, which give approximate analytical solutions, are widely used. With this motivation, in this thesis we study on BEC in stationary and rotating regimes using variational methods.

All the atoms in the condensate can be described with a single wave function, and in the dilute regime this wave function satisfies a single nonlinear equation (the Gross-Pitaevskii equation) which resembles the nonlinear Schrödinger equation in nonlinear optics. A simple analytical ansatz, which has been used to describe the intensity profile of the similariton laser [41, 43] having a similar behavior in the limiting cases of nonlinearity with ground state density profile of BECs, is used as the trial wave function to solve the Gross-Pitaevskii equation with variational principle for a wide range of the interaction parameter. The simple form of the ansatz allowed us to modify it for both cylindrically symmetric and completely anisotropic harmonic traps. The resulting ground state wave function and energy are in very good agreement with the analytical solutions in the limiting cases of interaction and numerical solutions for the intermediate regime.

In the second part, we consider a rapidly rotating two-component Bose-Einstein condensate containing a vortex lattice. We calculate the dispersion relation for small oscillations of vortex positions (Tkachenko modes) in the mean-field quantum Hall regime, taking into account the coupling of these modes with density excitations. Using an analytic form for the density of the vortex lattice, we numerically calculate the elastic constants for different lattice geometries. We also apply this method to the calculation the elastic constant for the single-component triangular lattice. For a two-component BEC, there are two kinds of Tkachenko modes, which we call acoustic and optical in analogy with phonons. For all lattice types, acoustic Tkachenko mode frequencies have quadratic wave-number dependence at long-wavelengths, while the optical Tkachenko modes have linear dependence. For triangular lattices the dispersion of the Tkachenko modes are isotropic, while for other lattice types the dispersion relations show directional dependence consistent with the symmetry of the lattice. Depending on the intercomponent interaction there are five distinct lattice types, and four structural phase transitions between them. Two of these transitions are second-order and are accompanied by the softening of an acoustic Tkachenko mode. The remaining two transitions are first-order and while one of them is accompanied by the softening of an optical mode, the other does not have any dramatic effect on the Tkachenko spectrum. We also find an instability of the vortex lattice when the intercomponent repulsion becomes stronger than the repulsion within the components.

Keywords: Bose-Einstein condensation, Gross-Pitaevskii equation, vortex lattice, Tkachenko modes, structural phase transition, phase separation, optical lattices.

ÖZET

DURAĞAN VE DÖNEN BOSE-EINSTEIN YOĞUŞMALARINA VARYASYONEL YAKLAŞIM

Murat Keçeli
Fizik, Yüksek Lisans
Tez Yöneticisi: Yrd. Doç. Dr. M. Özgür Oktel
Temmuz, 2006

Bose-Einstein Yoğuşması'nın (BEY'in) deneysel olarak gösterilmesinden sonra [6, 7, 18], ultrasoğuk atomik fizik hakkındaki deneysel ve kuramsal makalelerin sayısı hızla arttı [48]. Yapılan deneyler kuantum çok-parçacık sistemlerin kontrol edilebilmesini ve oldukça kesin ölçümler elde edilmesini sağladı. Buna ek olarak BEY fazında bağıntıların kuvvetli olması kuramsal olarak anlaşılmasını da diğer çok-parçacıklı kuantum sistemlerine göre kolay kılar. Bu güdülenme ile bu tezde BEY'i durağan ve dönen durumlarında varyasyonel yöntemler kullanarak kuramsal olarak inceledik.

Tezin ilk bölümünde durağan durum araştırıldı. BEY fazındaki atomlar tek bir dalga fonksiyonu ile ifade edilirler ve bu dalga fonksiyonu da doğrusal olmayan Gross-Pitaevskii denklemini sağlamak zorundadır. Bu denklem, daha önce similariton lazerlerinin yoğunluk profilini açıklamak için kullanılan fonksiyonun [41, 43] yardımıyla varyasyonel olarak çözüldü. Elde ettiğimiz sonuçlar sayısal yöntemlerle karşılaştırıldı.

Tezin ikinci bölümünde BEY fazına girmiş dönen gazlar incelendi. Bu fazdaki gazlar süperakışkan özellikleri gösterdikleri için hız alanları dönüşsüzdür. Dönmesi ancak belli bir açısal momentumun üzerinde oluşan girdaplarla mümkündür. Bu girdapların sayısı, dönme hızıyla beraber artar ve girdaplar bir örgü oluşturur. En düşük enerjili yapı süperiletkenlerdeki Abrikosov örgüsünde olduğu gibi üçgen örgüdür. Bu örgüdeki girdaplara ufak bir tedirginlik verildiğinde, örgü toplu olarak salınım yapar ve bu salınıma Tkachenko salınımı denir. Tezde önce tek bileşenli BEY'ler için bu salınımın hesaplanması gösterildikten sonra benzer yöntemi iki bileşenli beyler için uygulandı.

İki bileşenli BEY'lerin ilginç bir özelliği bileşenler arasındaki etkileşime bağlı olarak üçgen örgü dışında, kare, diktörtgen ve eşkenar dörtgen düzeninde örgüler oluşturabilmesidir. Tüm bu örgüler için Tkachenko salınımı frekansı hesaplanarak bu örgüler arasındaki faz geçişleri de incelendi. Elde edilen sonuçlara göre Tkachenko salınımının iki farklı kolu vardır. Bu kollar çift atomlu kristallerdeki fonon kipine benzetilerek, akustik ve optik kip diye adlandırıldı. Akustik kipin her örgü için yöne bağlı olduğu gösterildi. Bu da daha önce bu kipi araştırmak için yapılan deneyde bu salınımın hızla sönümlenişinin açıklanabilmesini sağladi. Ayrıca ikinci dereceden faz geçişlerinde akustik Tkachenko kipinin katı hal fiziğinden öngörülebileceği gibi yumuşadığı tespit edildi.

Anahtar sözcükler: Bose-Einstein yoguşması, Gross-Pitaevskii denklemi, girdap örgüleri, Tkachenko salınımları, faz geçişleri, yapısal faz ayrışması, optik örgüler.

Acknowledgement

First of all, I would like to express my deepest gratitude to my advisor Prof. Özgür Oktel for all his help throughout my thesis works. In our three years of study, he amazed me not only with his depth of knowledge but also with his kind personality. I would also like to thank Prof. Bilal Tanatar, for his guidance during my study in Bilkent. Moreover, I am grateful to Prof. Omer Ilday for the 'similariton' course project which turned into a chapter in this thesis. I also want to acknowledge Prof. Igor Kulik who has a great influence on me with his enthusiasm in physics.

I am also indebted to many friends in Bilkent as known as 'physgrad'. Among them, I should especially thank to Alper Duru, and our group members Sevilay Sevinçli, Emre Taşgın, Levent Subaşı, and Onur Umucalılar. Levent and Onur contributed to nearly all parts of this study. I have learned a lot from them, and I am also thankful to them for their invaluable friendship.

Finally, I want to thank to most special people for me, my parents, my sister Feyza and my fiancé Sevnur. I can not imagine a life without their love and support. This thesis can only be an opportunity for me to thank them, and as a part of my endless thanks, I want to dedicate this thesis to my mom and dad.

To my mom and dad...

Contents

List of Figures

List of Tables

Chapter 1

Introduction

If someone makes a survey about the most exciting topics in physics, the result will definitely include lasers, superconductors and superfluids. Bose-Einstein condensation (BEC) is in the heart of these three 'different' subjects. Lasers can be thought of as BEC of photons, superconductors are in a sense BEC of electron pairs and superfluids are composed of a condensed and a normal part. Therefore, it is very important to understand BEC to advance our knowledge about these topics.

Moreover, cooling below 10^{-6} K with the advanced laser and magnetic techniques has led to the demonstration of BEC in alkali atom gases, which was the holy grail of atomic physics. Although superconductors and superfluids can also be regarded as the experimental demonstration of BEC, the strong interaction and presence of noncondensed part in these systems shadow the simplicity and beauty of BEC. On the other hand, weak interaction among particles, and nearly 100% condensation in gaseous BEC is a clean demonstration of BEC phase. This provides a laboratory to test the theories of many-body quantum physics.

1.1 Bose-Einstein Condensation

In 1920s S.N. Bose, an Indian physicist from Bangladesh, was trying to publish his study about black-body radiation in which he treated electromagnetic waves as a gas of 'identical particles'. He wrote a letter to A. Einstein about his study and succeeded in attracting Einstein's interest and publishing his result [17]. Einstein extended the 'identical particle' approach to ideal gas and wrote the influential paper [28] in which he mentions about the critical point reached either decreasing the temperature or increasing the number of particles, where all the particles condense into ground state. Although it is not known at that time, this new statistics now called Bose-Einstein statistics is valid for bosonic particles which have integer spins.

For Bose-Einstein statistics, the distribution function, *average number of particles occupying single quantum state i*, can be derived using combinatorics and maximizing entropy for a microcanonical ensemble (total energy and number of particles are fixed);

$$f_i(\epsilon) = \frac{1}{e^{\beta(\epsilon_i - \mu)} - 1}, \tag{1.1}$$

where the physical meaning of β and μ can be understood from the first law of thermodynamics. It turns out that $\beta = 1/k_B T$ (k_B is Boltzmann constant and T is absolute temperature) and μ is the chemical potential, *the energy required to add a particle to the system.* The exponential term is also present in other distribution functions but the -1 term makes a difference. Absence of it leads to Maxwell-Boltzmann statistics and same term with opposite sign leads to Fermi-Dirac statistics which is for fermions.

The first order thermodynamic phase transition that Einstein pointed out occurs when the de Broglie wavelength $\lambda = \sqrt{2\pi\hbar^2/mk_BT}$ is as large as mean interparticle separation $r = n^{-1/3}$ ($\hbar, m, n$ are reduced Planck constant, particle mass, and number density, respectively). Critical temperature T_c is determined in the thermodynamic limit where the chemical potential is zero. Chemical potential is negative above this critical value and equals zero below T_c. This phenomenon did not create much attention until 1938 when superfluidity was discovered at a

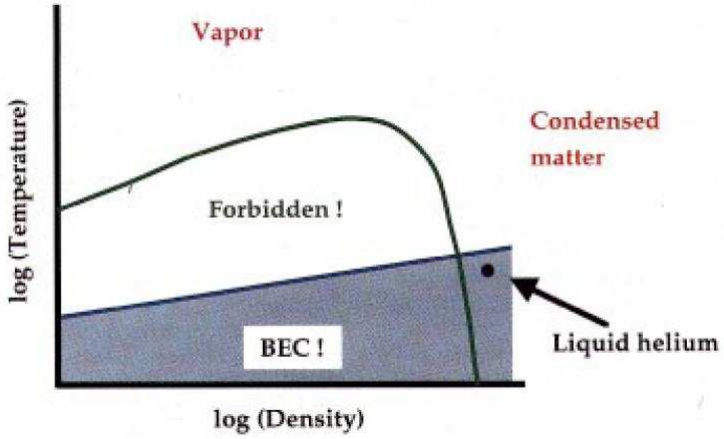

Figure 1.1: (Color) Phase diagram of ordinary matter. The region under the curve is forbidden. BEC of alkali gases is a metastable state in this region. From Fig. 4 of [22]

.

fairly close transition temperature for BEC (superfluid transition was observed for helium at 2.2 K whereas the critical temperature of BEC is 3.2 K). At that time F. London indicated this resemblance and BEC has started to be taken more seriously although the superfluid helium being a strongly interacting system differs from an ideal gas, and only 10% of the liquid is condensed [75].

Therefore, there was an enormous study to achieve BEC in a system that is close to an ideal gas. Although the idea is simple -*cool the gas until the de Broglie wavelength is close to interparticle spacing*- there are many experimental difficulties. Many groups in different countries try to capture this holy grail of atomic physics with different atoms like spin-polarized hydrogen, atomic hydrogen, sodium and rubidium. Main difficulty was the combination of molecules due to three body collisions and the formation of a solid instead of a BEC as can be seen from the phase diagram in Fig. 1.1. New techniques of cooling such as laser cooling and evaporative cooling with diluting the gas as much as 10^6 times thinner than air helped scientists a lot and finally in 1995 JILA group in Boulder, Colorado achieved BEC of 2000 Rb atoms. Soon after, the group of W. Ketterle at MIT demonstrated BEC of 10^6 Na atoms. These groups used a magnetic trap

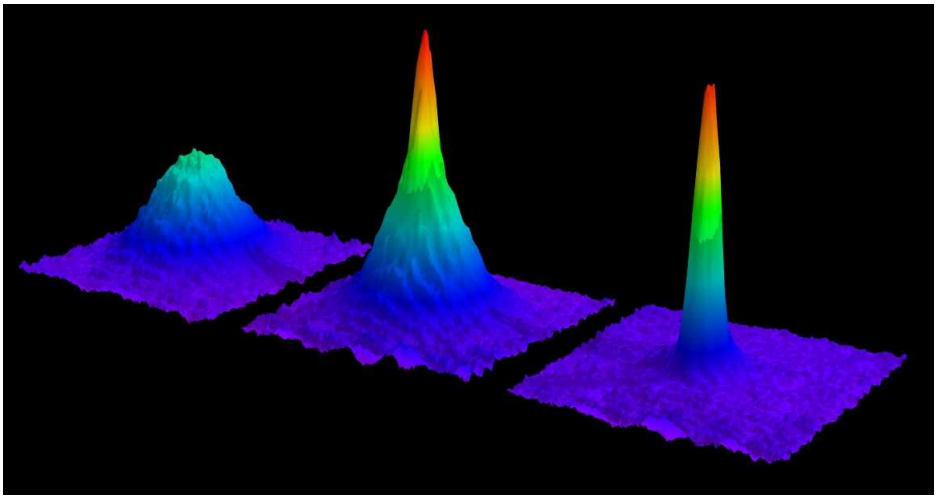

Figure 1.2: (Color) Images of velocity distributions from Ketterle group web site [1]. Leftmost image is taken at a temperature above T_c, the round Gaussian distribution is due to Maxwell-Boltzmann distribution. The middle image is just below the transition temperature where both thermal and condensed clouds are present, so there is a spike and a round curve. Right image is at a temperature $T \ll T_c$, so that the thermal cloud is vanishing and a peak comes from the atoms condensed at the ground state. Color corresponds to the number of atoms increasing from blue to red.

to hold the gas and were able to image it with optical methods. The clean evidence of BEC can be seen in the momentum distribution imaged after letting the gas expand. (Fig. 1.2)

Today, there are several experimental groups that run experiments on their BECs which can be created either by using magnetic, optical traps or even with permanent magnets (For more recent information see Ref. [2]). They can trap more than 10^6 atoms and cool down to temperatures beyond 10^{-9} K.

1.2 Organization of the Thesis

The thesis is organized as follows: Starting with a motivation and a brief introduction to Bose-Einstein Condensation, in Chapter 2 mean-field description of

BEC is given. The governing equation of BEC, the Gross-Pitaevskii equation, is introduced and possible solving methods are investigated. Following that a variational method to solve this equation is explained in detail. In the next chapter the effect of rotation on BEC is analyzed. This chapter is like a review of literature and an introduction to our main work in this thesis. The topological defects on BEC, vortices and vortex lattices are defined with the collective excitations of the lattice called Tkachenko oscillations. After that lowest Landau level regime and spinor condensates are introduced. Chapter 3 is the main work of this thesis and it is given in the same way as it is published. This work is about vortex lattice excitations in rotating spinor BECs. Inertial modes which are density oscillations are also derived but the main focus of interest is on Tkachenko modes. Since there are different lattice types in two-component BECs each lattice type and its excitation is investigated separately. The first and second order phase transitions between different lattice types are identified with the explanation of the related mechanism 'mode softening'. The summary of our results and possible extensions of this thesis are given in the concluding chapter.

Chapter 2

Gross-Pitaevskii Equation

As described in Section 1.1, below a critical temperature bosons occupy the ground state macroscopically. If the temperature is lowered continuously the condensate fraction increases and becomes one when $T = 0$. Since the experiments can be performed well below the critical temperature, one should not bother with the tiny uncondensed part. Assuming a pure condensate means that you can describe all the atoms in the system with a single wave function which simplifies the picture very much. However, since we still have a many body problem, we should consider the interaction between the particles.

Fortunately, BECs of alkali gases are very dilute, that is in the order of 10^{15} cm^{-3}, 10^6 times thinned with respect to air. This gives another simplification which is assuming only two body collisions. In fact, two body collisions are essential in producing BECs, because it restricts the possibility of atoms to form molecules which requires another atom to remove the excess energy of bonding. These type of collisions are described by s-wave scattering length a which can be determined experimentally. The typical values for alkali atoms are in the order of ten nanometers. These values can also be changed using magnetic field via Feshbach resonance. This brings a big freedom for theorists to interpret the interaction as they want. Although two-body collisions is a meaningful and helpful simplification, a nonlinear term which makes GPE analytically unsolvable is indispensable.

In this chapter, we will give a variational formulation of the Gross-Pitaevskii equation (GPE) in Section 2.1 and then give approximate analytical solutions for this equation in the following section. For the last section, we will solve GPE variationally using a trial wave function.

2.1 Mean Field Theory

Gross-Pitaevskii theory [62, 34, 35] is found to be very successful to describe the ground state and excitations of the Bose-Einstein condensates (BECs) in dilute atomic gases. The success of this theory lies in the fact that the condensate can be described with a single wave function and the interactions between the particles are described only with s-wave scattering. The condition for the former is $T \ll T_c$, where T_c is the critical temperature for BEC and for the latter is $n^{1/3}a \ll 1$, where n is the number density of the condensate and a is the s-wave scattering length. The theory reduces to a single equation that describes the condensate wave function, known as Gross-Pitaevskii equation (GPE); a type of nonlinear Schrödinger equation (NLSE) which arises in many areas of physics such as nonlinear optics (NLO) and hydrodynamic theory of fluids.

The energy functional for a condensate in a trap potential $V(\mathbf{r})$ can be written as,

$$E(\psi) = \int d\mathbf{r} \left(\frac{\hbar^2}{2m} |\nabla\psi(\mathbf{r})|^2 + V(\mathbf{r})|\psi(\mathbf{r})|^2 + \frac{g}{2}|\psi(\mathbf{r})|^4 \right). \tag{2.1}$$

The terms in the integral correspond to kinetic, trapping and interaction energies, respectively, where $g = \frac{4\pi\hbar^2 a}{m}$, and m is the atomic mass of the trapped bosons. GPE can be obtained by minimizing the ground state energy functional given in Eq. 2.1 of the condensate with respect to the wave function and complex conjugate of it. Time-independent GPE then follows as,

$$-\frac{\hbar^2}{2m}\nabla^2\psi(\mathbf{r}) + V(\mathbf{r})\psi(\mathbf{r}) + g|\psi(\mathbf{r})|^2\psi(\mathbf{r}) = \mu\psi(\mathbf{r}), \tag{2.2}$$

where μ is chemical potential introduced as the Lagrange multiplier with the normalization constraint $\int d\mathbf{r}|\psi(\mathbf{r})|^2 = N$. Normalization integral implies that

number density of the condensate is given as $n = |\psi(\mathbf{r})|^2$. Nonlinearity of GPE is due to interaction between particles and its effect becomes more pronounced as the number of particles in the condensate increases which is the case for current experiments where more than 10^7 particles are in the BEC phase. Since nonlinearity restricts exact analytical solutions of NLSEs except soliton-like solutions, many numerical algorithms [27, 63, 26, 64, 10] and variational methods [14, 42, 60, 32, 16, 65] are developed to find the ground state solution. Although variational methods give only an upper bound to the exact ground state energy, they require less calculation and can give accurate results if a suitable trial function is chosen. Another advantage of the variational principle is that it gives the functional form of the wave function which can be used to obtain further information on the condensate. Therefore, many trial functions are proposed for the purpose of obtaining a better bound for the ground state energy. These functions are generally chosen by adding parameters to a known approximate analytical solution and approximate solutions can be obtained by looking at the limiting cases of the GPE where the nonlinearity is negligibly small or very high.

2.2 Analytical Solutions

2.2.1 Ideal Gas Approximation

The nonlinearity in GPE arises from the interaction term and our first assumption will be to ignore this term. That is equal to assuming an ideal Bose gas. This leads to a linear equation, which is simply the Schrödinger equation where the chemical potential becomes the energy eigenvalue. However, this equation is exactly solvable for only very special potentials, so we will assume a spherical harmonic trap. This is not a bad approximation since this kind of trap is used in many experiments. Hence, the problem just turns into a simple quantum mechanics textbook example, a particle in a simple harmonic trap, and here we have N particles but they are all in the same state. This is exactly solvable and in

three dimensions the wave function has the form,

$$\psi(r) = \frac{\sqrt{N}}{\pi^{3/4} d^{3/2}} e^{-r^2/2d^2} \tag{2.3}$$

where d is the oscillator length, $d = \sqrt{\frac{\hbar}{m\omega}}$. Since this is the solution for noninteracting case, we can take it as our trial function to solve GPE given in Eq. (2.4) as a simple application of the variational method. We again assume a spherical harmonic trap, that is $V(r) = \frac{1}{2} m\omega^2 r^2$. Solving GPE is equivalent to finding the energy from Eq. (2.1) so by inserting the Gaussian wave function given in Eq. (2.3) as our trial function assuming the width of this Gaussian as our variational parameter, we can obtain,

$$E = \frac{3N}{4} \left(\frac{\hbar^2}{md^2} + m\omega^2 d^2 + \frac{4gN}{3(2\pi)^{3/2} d^3} \right). \tag{2.4}$$

We should minimize this energy with respect to d, our variational parameter, to find an equation for it. This gives us,

$$-\frac{\hbar^2 d}{m} + m\omega^2 d^5 - \frac{2gN}{(2\pi)^{3/2}} = 0. \tag{2.5}$$

This equation is a fifth order polynomial equation, so it doesn't have a closed form solution. Therefore, we should solve it numerically. Inserting, $g = \frac{4\pi\hbar^2 a}{m}$ where a is the s-wave scattering length which is a quantity that can be tuned using the Feshbach resonance ideally from $-\infty$ to ∞, and scaling the parameter d with the oscillator length, we get

$$-\tilde{d} + \tilde{d}^5 - \tilde{g} = 0, \tag{2.6}$$

where $\tilde{g} = \sqrt{\frac{2m\omega}{\pi\hbar}} aN$ and $\tilde{d} = \frac{d}{\sqrt{\frac{\hbar}{m\omega}}}$.

As a check we can easily see the solution for $\tilde{g} = 0$ gives $\tilde{d} = 1$ which is the solution for the ideal gas case. We can find the solutions for different values of $\tilde{g}$ and obtain the density profiles for these different regimes.

2.2.2 Thomas-Fermi Approximation

For the opposite case where nonlinearity is dominant, the kinetic energy term can be neglected in GPE, which is called Thomas-Fermi Approximation (TFA).

If we write GPE given in Eq. 2.2 without this term, we get,

$$V(\mathbf{r})\psi(\mathbf{r}) + 2g|\psi(\mathbf{r})|^2\psi(\mathbf{r}) = \mu\psi(\mathbf{r}). \tag{2.7}$$

We can easily see that solution for the density is,

$$n(\mathbf{r}) = \frac{\mu - V(\mathbf{r})}{2g} \tag{2.8}$$

when right hand side of the equation is positive, and zero otherwise. Since the chemical potential and interaction strength does not depend on the position we can say that density profile is determined by the trapping potential. Hence if we have a harmonic trap as in the previous case the density profile turns out to be an inverted parabola. This shows that as the interaction increases the density profile changes from a Gaussian to a parabola for a harmonic trap. TFA can be improved by adding the kinetic energy term obtained with the resulting wave function. However, derivative of the resulting wave function has logarithmic divergence which forces a cut off radius R to be inserted to improve the approximation. This gives kinetic energy per particle as [52],

$$\frac{E_{kin}}{N} = (15\beta)^{-2/5}\left(\frac{1}{2}\ln(480\beta) - \frac{5}{4}\right), \tag{2.9}$$

where $\beta \equiv Na/a_\omega$ is known as the interaction parameter.

2.2.3 Similariton Ansatz for variational calculations [45]

Recently a semi-analytic theory of the similariton lasers is developed [43] using a trial pulse shape which can be adjusted to have either a Gaussian or a parabolic form. The trial function to describe the intensity profile is given as,

$$S_n(x) = \exp\left(-\sum_{k=1}^{n}\frac{x^{2k}}{k}\right). \tag{2.10}$$

For this function, the Gaussian to parabolic behavior can be clearly seen in Fig. 2.1 as the parameter n changed. In nonlinear optics (NLO) the intensity of light is analogous to the density of the condensate and NLSE for this system is used to describe the propagation of laser light in an optical medium where the nonlinearity gets in. Since the governing equations are very similar, it is natural to expect

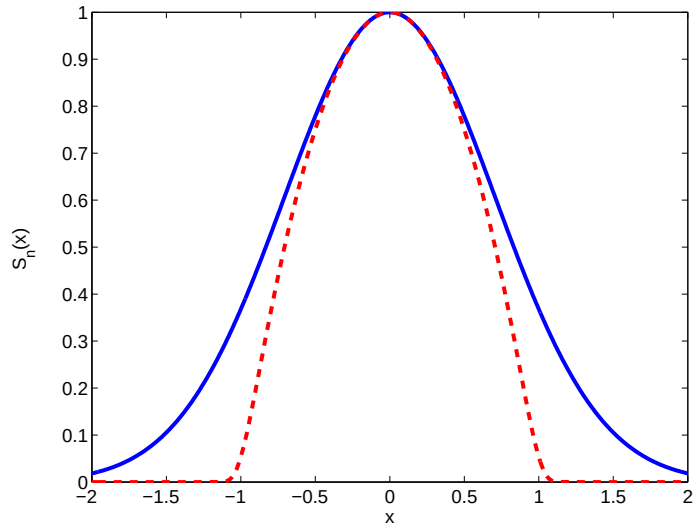

Figure 2.1: Trial similariton function. Solid curve is for $n = 1$ and dashed curve is for $n = 10$.

similar solutions for these different systems. Soliton-like solutions and self-similar solutions (SSS) of NLSE are important both in BEC and NLO. Soliton-like solutions arise when the nonlinearity is compensated by the dispersion, and they are only exact analytical solutions of these NLSEs, whereas self-similar solutions are asymptotic solutions that show up when the effects of initial conditions die out, but the system is still far from the final state [11]. Although soliton type solutions are well investigated in both NLO and BEC communities, SSS are not well studied. In BEC community self-similar solutions are used to understand BEC growth when the the trap holding the condensate is removed. In optics, these type of solutions are used more extensively from Raman scattering to pulse propagation in fibers, and it is shown that linearly chirped parabolic pulses are exact asymptotic solutions of NLSE with gain [41]. Recently, self-similar propagation of ultrashort parabolic pulses in a laser resonator is observed and an analytic ansatz is developed to describe the intensity profile of this pulse [43]. The so called 'similariton' pulse has a nearly parabolic intensity profile to reduce the effect of Kerr nonlinearity. However, initially nonlinearity is lower and the pulse has a Gaussian shape. Therefore, the ansatz proposed in [43] to describe these pulses has an adjustable profile between a Gaussian and an inverted parabola which is given in Eq. (2.10).

This function becomes a Gaussian when $n = 1$ and turns into an inverted parabola when $n \to \infty$ since the summation in the exponent converges to $\ln(1 - x^2)$ in that limit for $|x| < 1$, moreover it converges so quickly that adding about ten terms is enough to get a parabolic profile with smoother ends which is a desirable property. Besides, this function is integrable which makes it a good candidate for variational calculations.

For the reasons explained, we will make use of the similariton ansatz given in Eq. 2.10 as our trial wave function to minimize the energy functional given in Eq. (2.1). To simplify the calculations, we nondimensionalize the Gross-Pitaevskii functional by scaling length, energy and wave function with oscillator length $a_\omega = \sqrt{\frac{\hbar}{m\omega}}$, $\hbar\omega$ and $\sqrt{Na_\omega}$, respectively. We first analyze the solution for spherical harmonic trap $V(r) = \frac{1}{2}m\omega^2 r^2$ and introduce the parameter $\beta \equiv Na/a_\omega$ which is a measure of the influence of the interaction.

$$\frac{E(\psi)}{N} = 2\pi \int_0^\infty d^3r \left(|\nabla\psi(r)|^2 + V(r)|\psi(r)|^2 + 2\pi\beta|\psi(r)|^4 \right). \tag{2.11}$$

Ideally β can take any value between $-\infty$ to ∞ since all the parameters inside are experimentally tunable. However, negative scattering length which means attractive interaction, causes collapse of the condensate when the particle number is high. For this regime our results agree with the results given in Ref. [14]. In the present work we concentrate on repulsive interaction. With proper normalization the trial wave function has the form,

$$\psi(r) = \sqrt{\frac{1}{4\pi d^3 I_n}} \exp\left(\sum_{k=1}^{n} \frac{(r/d)^{2k}}{2k} \right), \tag{2.12}$$

where d and n are our variational parameters with $I_n = \int_0^\infty dr r^2 p_n(r)$ which is an integral that can be calculated analytically for $n = 1, 2$ and numerically for $n > 2$. Here the parameter d is responsible for the width of the condensate which increases as the interaction increases, and n takes care of flattening of the central density. We minimize the energy with respect to d for different n values and chose the n that gives the minimum energy. For d, we obtain a fifth order polynomial equation where only one of the roots is physically meaningful.

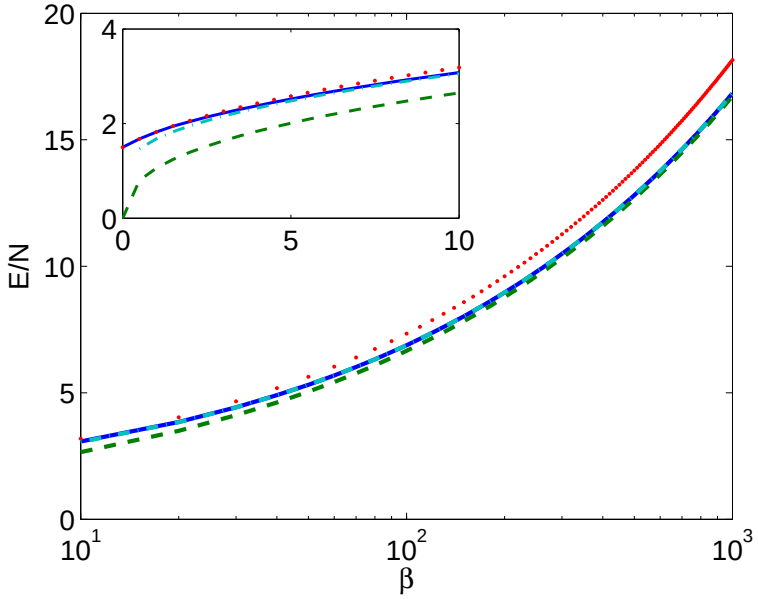

Figure 2.2: (Color) Ground state energy with respect to interaction parameter β obtained with the variational function (black solid line). The resulting energy of a Gaussian variational function is given with dotted (red) line and energy obtained with Thomas-Fermi solution is given with dashed line (green). Improved Thomas-Fermi solution [52] is given with dotted line (blue). The inset is given for small β values.

2.2.3.1 Isotropic Traps

We can compare our results with the analytical approximations. For small β values, our trial function reduces to a Gaussian and gives the exact result for $\beta = 0$, and for large β our results agree well with the improved TFA results as shown in Fig. 2.2. We also compared the resulting wave function with the numerical solutions obtained by steepest descent method (with courtesy of S. Sevinçli) for different β values in Fig. 2.3. We also tabulated our results in Table 2.1 and include the results of a recent numerical analysis which direct minimizes the energy functional by the finite element method. Here it should be noted that tabulated kinetic, trap, and interaction energies satisfy the virial theorem which foresees the relation $2E_{kin} + 2E_{pot} - 3E_{int} = 0$. It is also remarkable that even for large β adding 10 terms is enough to find the wave function (see Fig. 2.4) which shows the easiness of the calculations.

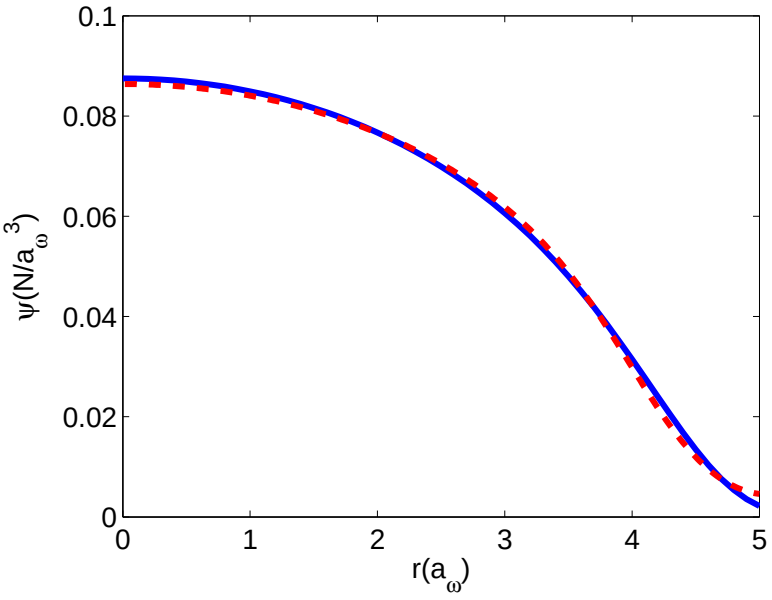

Figure 2.3: (Color) Wave function calculated with the steepest descent method [26] is shown with bold line (blue) whereas the similariton ansatz solution is given with dashed line (red) for $\beta = 100$.

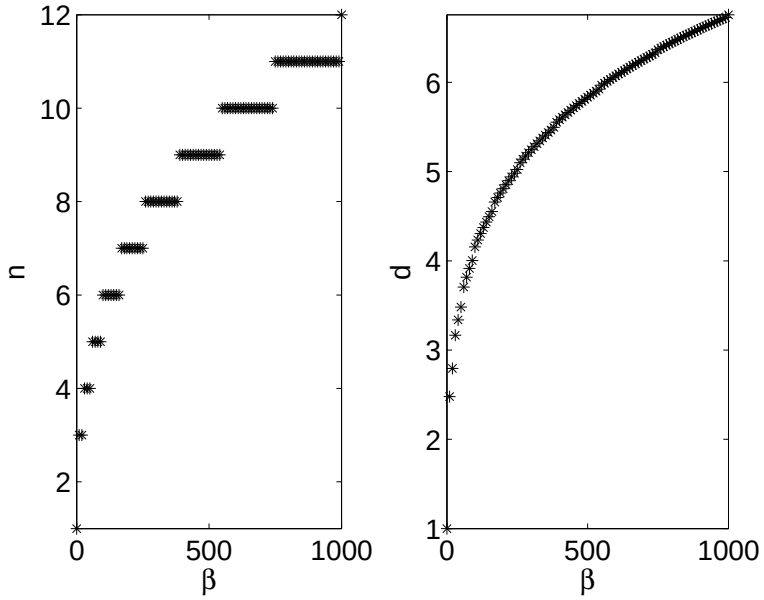

Figure 2.4: Change of variational parameters with interaction parameter β is given. Left plot shows the number of terms in the summation and the right one shows the change of width of the similariton ansatz.

Table 2.1: The value of the wave function at the center, the root mean square size r_{rms} and chemical potential is tabulated in units of $\sqrt{N/a_w^3}$, a_w and $\hbar\omega$ respectively. For comparison numerical results of Ref. [10] is given in parentheses.

β	$\psi(0)$	r_{rms}	μ
0	0.4238 (0.4238)	1.2248 (1.2248)	1.5000 (1.5000)
0.2496	0.3969 (0.3843)	1.2794 (1.2785)	1.6805 (1.6774)
0.9986	0.3475 (0.3180)	1.3981 (1.3921)	2.0885 (2.0650)
2.4964	0.2515 (0.2581)	1.5355 (1.5356)	2.5803 (2.5861)
9.9857	0.1739 (0.1738)	1.8822 (1.8821)	4.0089 (4.0141)
49.926	0.1097 (0.1066)	2.5071 (2.5057)	7.2576 (7.2484)
249.64	0.0665 (0.0655)	3.4152 (3.4145)	13.559 (13.553)
2496.4	0.0330 (0.0328)	5.3855 (5.3852)	33.812 (33.810)

2.2.3.2 Cylindrical Traps

Using similar trial functions, we can also solve the GPE for cylindrical and fully anisotropic traps. For the cylindrically symmetric trap, trial function takes the form,

$$\psi(\rho, z) = C \exp(-\sum_{k=1}^{n_\rho} \frac{(\rho/d_\rho)^{2k}}{2k}) \exp(-\sum_{k=1}^{n_z} \frac{(z/d_z)^{2k}}{2k}), \tag{2.13}$$

where, $C = \sqrt{\frac{N}{2\pi {d_{ro}}^2 d_z I_\rho I_z}}$,$I_\rho = \int_0^\infty \rho d\rho S_n(\rho)$ and $I_z = \int_{-\infty}^{\infty} dz S_n(z)$. We have four variational parameters, but calculations are similar to the isotropic case. We compared our results with the numerical results of Dalfovo *et al* [26] in Table 2.2. The cylindrically symmetric traps are the most common one in BEC setups and aspect ratio obtained from $\frac{x_{rms}}{z_{rms}}$ is very important to identify the BEC phase in these experiments. It is shown in [14, 26] that for the noninteracting case this ratio is equal to $\sqrt{\lambda}$, and goes to λ in the Thomas-Fermi limit. This result is clearly seen from the values in Table 2.2 where $\lambda = \sqrt{8}$ and it is also evident that convergence of TFA is very slow.

Table 2.2: Results of our calculation for a cylindrically harmonic trap with $\lambda = \sqrt{8}$. Energy and length units are $N\hbar\omega$ and a_ω. The results of the numerical calculation in Ref. [26] is given in parentheses for comparison except for the last row. For $\beta = 2165$ Thomas-Fermi result for the chemical potential are given in parentheses.

β	x_{rms}	z_{rms}	E_{kin}	E_{tr}	E_{int}	μ
0.0000	0.7071 (0.707)	0.4204 (0.42)	1.2071 (1.207)	1.2071 (1.207)	0.0000 (0.000)	2.4142 (2.414)
0.4330	0.7901 (0.79)	0.4374 (0.44)	1.0539 (1.06)	1.3894 (1.39)	0.2237 (0.21)	2.8907 (2.88)
0.8660	0.8500 (0.85)	0.4472 (0.45)	0.9976 (0.98)	1.5225 (1.52)	0.3500 (0.36)	3.2200 (3.21)
2.1650	0.9657 (0.96)	0.4707 (0.47)	0.8528 (0.86)	1.8188 (1.81)	0.6440 (0.63)	3.9596 (3.94)
4.3300	1.0892 (1.08)	0.4966 (0.50)	0.7337 (0.76)	2.1730 (2.15)	0.9595 (0.96)	4.8258 (4.77)
8.6600	1.2319 (1.23)	0.5332 (0.53)	0.6709 (0.66)	2.6549 (2.64)	1.3227 (1.32)	5.9712 (5.93)
21.650	1.4798 (1.47)	0.5930 (0.59)	0.5314 (0.54)	3.5963 (3.57)	2.0432 (2.02)	8.2142 (8.14)
43.300	1.7038 (1.69)	0.6536 (0.65)	0.4351 (0.45)	4.6121 (4.57)	2.7847 (2.74)	10.616 (10.5)
64.950	1.8447 (1.84)	0.6989 (0.70)	0.4128 (0.41)	5.3569 (5.31)	3.2960 (3.26)	12.361 (12.2)
86.600	1.9562 (1.94)	0.7319 (0.73)	0.3789 (0.38)	5.9693 (5.91)	3.7270 (3.68)	13.802 (13.7)
2165	3.7367	1.3297	0.1459	21.035	13.926	49.033

2.2.3.3 Completely Anisotropic Traps

There are also experiments with fully anisotropic traps [50] and for this case the trial function assumes the form,

$$\psi(x,y,z) = C\exp\left(-\sum_{k=1}^{n_x,n_y,n_z}\frac{(x/d_x)^{2k}+(y/d_y)^{2k}+(z/d_z)^{2k}}{2k}\right), \tag{2.14}$$

where it has six parameters and C is the normalization constant. The results are given in Table 2.3 where the agreement with the results in [64] is apparent.

Table 2.3: The chemical potential per particle in units of $\hbar\omega$ is calculated using the ansatz given in Eq. (2.14) for a completely anisotropic trap with $\lambda = \sqrt{2}$ and $g\gamma = 2$. The interaction parameter β is obtained from Ref. [50] and the values in parentheses corresponds to the numerical solution given in [64]. The variational parameters $n_{x,y,z}$ and $d_{x,y,z}$ are also tabulated.

β	n_x, d_x	n_y, d_y	n_z, d_z	μ
0	1 , 1.000	1 , 0.840	1 , 0.707	2.207 (2.207)
1.787	2 , 1.753	2 , 1.368	1 , 0.817	3.604 (3.572)
3.575	2 ,1.956	2 , 1.489	2 , 1.160	4.385 (4.345)
7.151	3 , 2.433	2 ,1.654	2 , 1.258	5.492 (5.425)
14.302	3 , 2.780	3 , 2.035	2 , 1.384	7.010 (6.904)
28.605	4 , 3.310	3 , 2.30	3, 1.687	9.049 (8.900)
57.211	5 , 3.880	4 , 2.725	3 , 1.896	11.78 (11.57)

Chapter 3

Rotating Bose-Einstein Condensates

The most important characteristics of superfluids arises when they are set to rotating. Interestingly, these quantum fluids resist to rotating, since the velocity field of superfluids is irrotational due to macroscopic wave function describing it. However, above a critical rotation frequency a vortex appears which carries the angular momentum of the system, and as the rotation frequency is increased more vortices enter the system. These vortices form a regular lattice because of mutual repulsion in between. In this chapter we start with the definition of a vortex and in the following sections we define vortex lattices and collective vortex lattice excitations, which are called Tkachenko modes. In Section 3.2 we concentrate on the lowest Landau level regime where the rotation frequency is close to trapping frequency. We finish the chapter with the discussion of spinor condensates.

3.1 What is a Vortex?

Vortex formation is seen in superconductors, superfluids and atomic BECs. They are basically angular momentum carriers of the system where the density of the system goes to zero. We can see how they are formulated in the following

manner. Defining the condensate wave function 'order parameter' as

$$\Psi(\mathbf{r},t) = |\Psi(\mathbf{r},t)|\, e^{i\phi(\mathbf{r},t)} \tag{3.1}$$

Hence, we can define the velocity of the condensate as;

$$\mathbf{v}(\mathbf{r},t) = \frac{\hbar}{M}\nabla\phi(\mathbf{r},t) \tag{3.2}$$

From the above expression we can immediately see that the curl of the condensate is zero, meaning that motion of the condensate is restricted that the flow velocity is irrotational. The only exception happens if the phase of the order parameter has a singularity. We also know that order parameter should be single valued, so around a closed contour the change in the phase should be a multiple of 2π.

$$\Delta\phi = \oint d\mathbf{l}\cdot\nabla\phi = 2\pi l, \tag{3.3}$$

By defining the circulation Γ around a closed contour as

$$\Gamma = \oint d\mathbf{l}\cdot\mathbf{v} = l\frac{h}{M}, \tag{3.4}$$

We can also find velocity using the circulation,

$$v = l\frac{h}{2\pi r M} \tag{3.5}$$

By the aid of Stokes' theorem

$$l\frac{h}{M} = \int d\mathbf{S}\cdot\nabla\times\mathbf{v} \tag{3.6}$$

Thus, curl of velocity is more generally;

$$\nabla\times\mathbf{v} = l\frac{h}{M}\,\delta^{(2)}(x,y)\;\hat{\mathbf{z}}. \tag{3.7}$$

So we see that vortices (here one vortex at (0,0)) are the singularities where all the rotation is concentrated. A point vortex is the picture in two dimensions. In three dimensions vortices are lines called vortex filaments. We can think of a vortex as the quantum of angular momentum and it contains a phase singularity at its core around which 2π multiple of phase winding occurs. These winding allows rotation and coriolis force leaves the core fluidless [20]. The other interesting property of vortices is that because of the repulsive interaction in between

they form regular arrays as rotation rate is increased. For a single-component condensate, the form is hexagonal lattice which is similar to the Abrikosov lattice [5] seen in superconductors. In a two-component condensate the form turns out to be a square lattice. If the two components are prepared from the internal spin states of the same atom, the vortices of either components are filled by the other component forming a Skyrmion lattice [57].

3.2 Vortex Lattices and Lowest Landau Level

For an axially symmetric system with one vortex at center, each particle carries an angular momentum of $l\hbar$ where l is an integer. If $l = 1$, vortex is called singly quantized, and it turns out that doubly or more quantized vortices are not energetically favorable. Therefore, as more angular momentum is given to the system, more singly quantized vortices appear in the fluid, and due to repulsive interaction between these vortices, they form a regular lattice. As Tkachenko showed in 1966 [70] the lowest energetic form of this array is the triangular lattice as in the case of Abrikosov lattice in type II superconductors. The vortex lattice thus formed also rotates with the system like a classical body as expected from the correspondence principle since angular momentum is very high. (Fig. 3.1) The parabolic density profile is also seen in rotating condensates with vortex lattices as in the classical rotating fluids.

Although increasing number of vortices can carry as much angular momentum as you can give to the system, there is a limit for the rate of rotation, which is determined by the trapping frequency. This is a natural limit because above this speed the atoms of the gas starts to fly out from the trap due to centrifugal force. From the theoretical point of view, this limit is as much interesting as it is hard to be achieved experimentally. It is interesting because the physics of this regime resembles quantum Hall physics and it is hard to be achieved because of the difficulty of keeping the condensate in the trap. Fortunately new experimental methods like evaporative spin up technique allowed scientists in Boulder to achieve 99.9% of the trapping frequency and up to 200 vortices are

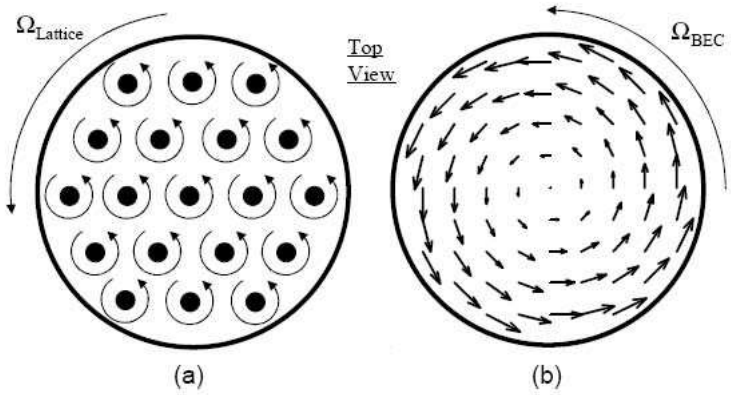

Figure 3.1: (a) Vortex Lattice (b) Classical body rotation ([36])

observed [73].

Landau levels are known to be the energy levels of charged particles under magnetic fields. In the limit of fast rotation single particle Hamiltonian resembles to Hamiltonian of these particles. If we move to the rotating frame (with Ω), the single particle Hamiltonian in the transverse direction becomes,

$$H = \frac{p_x^2 + p_y^2}{2m} + \frac{1}{2}m\omega_\perp^2(x^2 + y^2) - \Omega L_z + gn \tag{3.8}$$

Defining the vector potential as $\mathbf{A} = \mathbf{m\Omega} \times \mathbf{r}$ and neglecting the interaction term, Eq. 3.8 turns into,

$$H = \frac{\mathbf{p}_\perp - \mathbf{A}}{2m} + \frac{1}{2}m(\omega_\perp^2 - \Omega^2)(x^2 + y^2), \tag{3.9}$$

which is just the Hamiltonian of a $-e$ charged particle under a magnetic field $2m\Omega$ perpendicular to xy plane with a harmonic trap frequency $\sqrt{\omega_\perp^2 - \Omega^2}$. This system has the energy eigenvalue,

$$E_{m,n} = \hbar[\omega_\perp + n(\omega_\perp + \Omega) + m(\omega_\perp - \Omega)]. \tag{3.10}$$

This gives the energy bands shown in Fig. 3.2 when $\frac{\omega_\perp - \Omega}{\omega_\perp} \ll 1$. Since the density is very thin at this rotation frequency the condition of $gn \ll 2\hbar\omega_\perp$ is

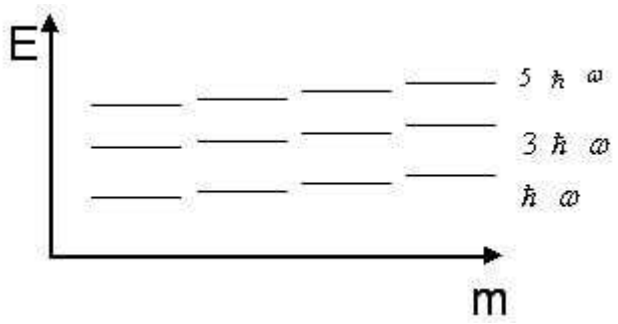

Figure 3.2: Energy bands in the LLL regime. $n = 0$ is the lowest energy and n increases in the vertical direction. Infinite degeneracy of m in Landau levels is lifted because of the minute difference between rotation frequency and trapping frequency.

easily satisfied where $2\hbar\omega_\perp$ is the energy spacing between the bands. This leads to condensation in the lowest Landau levels $n = 0$. The advantage of this level is that the wave function can be written analytically. The wave function is a gaussian multiplied by an analytic function,

$$\psi(x, y) = e^{-r^2/2a_\perp^2} A(x + iy) \tag{3.11}$$

where $a_\perp$ is the harmonic oscillator length. Since the roots of the analytic function A has complex roots with 2π phase change around it, they define the positions of vortices. Making the LLL approach one can calculate the energy of the vortex lattice precisely, if one knows the positions of the vortices. The details of LLL calculations are given in Appendix A.

3.3 Tkachenko Oscillations

We have seen above that when a BEC rotates faster than a critical frequency a vortex forms in the condensate, and as we increase the rotation frequency further new vortices will form and these vortices form regular triangular arrays. In 1966 V. K. Tkachenko showed the stability of the triangular vortex lattice [70] and he also he investigated effects of small perturbations on this lattice. Eventually he derived the dispersion law for lattice oscillations and concluded that at long wavelengths they resemble transverse sound in crystals [71]. He calculated

the shear modulus of the lattice in the superfluid resulting from the stiffness of the triangular array [72]. The shear modulus determines the spectrum of Tkachenko waves. This soft mode of vortex lattice is basically elliptical motion of vortex cores around their stable positions. In the calculations, Tkachenko used elasticity theory for two dimensional vortex array, and his results could not be derived from Bekarevich-Khalatnikov hydrodynamics due to ignorance of the energy increase produced by shearing of the vortex lattice. Lately G. Baym and E. Chandler reformulated hydrodynamics equations to include elasticity [13].After that E. B. Sonin considered the compressibility of the fluid in his calculations[67] and derived Tkachenko modes as well as other modes sustained by the lattice. Indeed there are three classes of compressional modes; transverse, longitudinal, and differential longitudinal. Experiments on rotating BECs has increased the interest in Tkachenko methods and led to both analytical and numerical studies. Although the predictions are close to the experimental data, theory is not complete. Here, we will follow the procedure of Baym and Chandler to derive the dispersion relation for Tkachenko mode. The picture in the reference [13] is two dimensional. We can define the vortex lattice as;

$$\mathbf{r}_{ij}^{0} = i\mathbf{a} + j\mathbf{b} \tag{3.12}$$

where a and b denotes the translation vectors of the lattice. When the vortex is slightly perturbed new position can be defined via the deformation vector.

$$\boldsymbol{\epsilon}_{\mathbf{ij}} = \mathbf{r}_{\mathbf{ij}} - \mathbf{r}_{\mathbf{ij}}^{\mathbf{0}} \tag{3.13}$$

For a non dissipative flow of a rotating superfluid we can write the continuity equation in the laboratory frame as

$$\frac{\partial \rho}{\partial t} + \nabla \cdot \mathbf{j} = 0 \tag{3.14}$$

where we have used of the hydrodynamic equations

$$\mathbf{j} = (\rho - \rho)\mathbf{v} + \rho^{*}\dot{\epsilon} \tag{3.15}$$

$$\frac{\partial j_i}{\partial t} + \frac{\partial \left[(\rho - \rho)v_i v_k + \rho^{*}\dot{\epsilon}_i\dot{\epsilon}_k\right]}{\partial t} + \frac{\partial}{\partial r_i}P + \sigma_{el,i} = 0 \tag{3.16}$$

$$\sigma_{el,i} = \frac{\hbar\Omega_0}{4m}\rho[2\nabla_i(\nabla\cdot\epsilon) - \nabla^2\epsilon_i] \tag{3.17}$$

$$\frac{\partial \mathbf{v}}{\partial t} + (\nabla \times \mathbf{v}) \times \dot{\epsilon} = -\nabla(\mu + v^2/2) \tag{3.18}$$

We can write these equations also in a frame rotating with Ω_0 and then linearize them, obtaining

$$\frac{\partial \rho}{\partial t} + (\rho - \rho)\nabla \cdot \mathbf{v} + \rho^* \nabla \cdot \dot{\epsilon} = 0 \tag{3.19}$$

$$\frac{\partial \mathbf{j}}{\partial t} + 2\mathbf{\Omega_0} \times \mathbf{j} + \nabla P' + \sigma_\mathbf{e} \mathbf{l} = 0 \tag{3.20}$$

$$\frac{\partial v}{\partial t} + 2\mathbf{\Omega_0} \times \dot{\epsilon} = -\nabla \mu' \tag{3.21}$$

where $\mu' = \mu - (\mathbf{\Omega_0} \times \mathbf{r})^2/2$ is the reduced chemical potential and $P' = P - \rho \mathbf{\Omega_0} \times \mathbf{r}^2/2$ is the reduced potential. These equations describe two dimensional flow of a rotating superfluid where the vortex line bending effects are ignored. These equations with the equation of state $P(\rho)$ form a system of six first-order equations for $\mathbf{v}, \epsilon, \dot{\epsilon}$ and ρ. We can find Tkachenko mode from these equations by neglecting ρ^* and considering an incompressible fluid with $\frac{\partial \rho}{\partial t} = 0$ (valid for superfluid He and slowly rotating BECs). Then we get,

$$\nabla \cdot \mathbf{v} = 0 \tag{3.22}$$

$$\frac{\partial v}{\partial t} + 2\mathbf{\Omega_0} \times \dot{\epsilon} = -\nabla \mu' \tag{3.23}$$

$$\frac{\partial v}{\partial t} + 2\mathbf{\Omega_0} \times \mathbf{v} = -\nabla \mu' - \sigma_e l/\rho \tag{3.24}$$

We can get rid of v and reduce the equations to two;

$$\frac{\partial^2}{\partial t^2}(\nabla \times \epsilon)_z + \left(\frac{\hbar}{8m}\nabla^2 + 2\Omega_0\right)\frac{\partial}{\partial t}\nabla \cdot \epsilon = 0 \tag{3.25}$$

$$\frac{\partial}{\partial t}(\nabla \cdot \epsilon) + (\frac{\hbar}{8m}\nabla^2)(\nabla \times \epsilon)_z = 0 \tag{3.26}$$

Now it is easy to obtain the solution by substituting $\epsilon = \epsilon_0 \exp i\mathbf{k} \cdot \mathbf{r} \exp -i\omega t$ in the long wavelength limit $k \to \infty$.

$$\omega_T = \sqrt{\frac{\hbar \Omega_0}{4m}} k \tag{3.27}$$

The displacement vector ϵ rotates around an ellipse whose major axis is perpendicular to and minor is along the vector $\mathbf{k}$.

3.4 Spinor Condensates

We have seen that a single-component BEC forms an Abrikosov lattice when it is set rotating. Long wavelength excitations and static properties of this type are well studied [53, 3, 38, 39, 19, 73]. A more interesting case is to study the multi-component condensate. A multi-component condensate can be created using either different species, or different internal states of the same atoms. In the single-component case spin degree of freedom played no role. By considering the internal spin states of an atom we can create a multi-component condensate which is called spinor condensates. The advantage of having the mixture of internal states of the same atom is that there can be controllable transition from one state to another whereas for the condensate of two different species you don't have such an opportunity. But we lose the conservation of number of particles because of these transitions [61].

One of the best candidates that can be used for a double-condensate experiment is ^{87}Rb. Applied magnetic field splits ^{87}Rb ground state into eight states due to hyperfine and Zeeman effects. Among the eight, only three of the states ($|F = 1, m = -1\rangle$,$|F = 2, m = 1\rangle$, $|F = 2, m = 2\rangle$) can be magnetically trapped, and two of the three has fairly equal magnetic moments so that they can be confined in an overlapping TOP trap. The states labelled $|1\rangle$ is $|F = 1, m = -1\rangle$, and $|2\rangle$ is $|F = 2, m = 1\rangle$ are the suitable ones for trapping.

First realization of vortices in a BEC was a spinor double-condensate experiment realized again by JILA group [55]. In the experiment they used ($|F = 1, m = -1\rangle$, and $|F = 2, m = 2\rangle$ states of ^{87}Rb.

Chapter 4

Spinor BECs in the Lowest Landau Level

This chapter is the main focus of our thesis and it is given here as it is published [46].

One of the defining properties of superfluidity is that a superfluid responds to rotation by forming quantized vortices. Generally, instead of forming multiply quantized vortices, it is more favorable for a superfluid to create many singly quantized vortices and arrange them in a vortex lattice. Since the original predication of such structures by Abrikosov [5], vortex lattices have been observed in type-II superconductors [30], superfluid helium [76], Bose-Einstein condensed gases (BECs) [37, 4] and most recently in ultracold fermion superfluids[78].

Once a vortex lattice is formed in a superfluid, small deviations of the vortices from their equilibrium positions require relatively small energy compared to other hydrodynamic modes of the system, and collective behavior of such small deviations result in a low-energy branch in the excitation spectrum. The modes on this branch, which were studied by Tkachenko in the context of superfluid helium [70, 71, 72], are called Tkachenko modes and in a simplified picture can be thought of as phonons of the vortex lattice. Tkachenko modes strongly affect the dynamics of the superfluid [13], and play an important role in many different

problems, ranging from vortex melting [66] to neutron star glitches [54].

Recent experiments on ultracold atoms have been successful in creating large vortex lattices in rotating harmonically trapped BECs [37, 4]. Remarkable results about vortex dynamics have been obtained, including the observation of Tkachenko modes over a large range of rotation frequencies [19]. In this experiment, after the formation of the vortex lattice, a resonant laser beam was focused on the center of the condensate to excite the Tkachenko modes and subsequently their frequency was measured. As the rotation frequency is increased, a clear reduction in the Tkachenko mode frequencies is observed.

Theoretical study of Tkachenko modes of trapped BECs has been carried out by a number of groups [25, 12, 69, 24, 68, 23, 8, 56]. In particular, the effects of finite size of the vortex lattice and the compressibility of the BEC lead to major differences in the Tkachenko spectrum compared with the Tkachenko modes of an incompressible superfluid such as helium. As the rotation frequency of the cloud is increased, the compressibility of the BEC starts to play an important role, reducing the shear modulus of the vortex lattice and thus the Tkachenko mode frequencies. When the rotation frequency Ω becomes close to the chemical potential $\mu = gn$, the gas enters the mean-field quantum Hall regime [40] where only the states in the lowest Landau level (LLL) are populated. Here, the trend of decrease in Tkachenko frequencies continues. As the rotation frequency Ω gets closer to the trapping frequency ω, more vortices enter the system, and mean-field description breaks down at the point where the number of vortices is comparable to the number of particles [66]. In the strongly correlated regime, the vortex lattice is expected to melt into a vortex liquid and subsequently go through a sequence of quantum Hall states ending with the Bosonic Laughlin state when $(\omega - \Omega)/\omega \sim 1/N$, with N being the number of particles [21].

In the experiments of the JILA group, rotation frequencies up to 99% of the trapping frequency have been achieved [74] and a calculation of the Tkachenko frequencies in the mean-field quantum Hall regime [12] found good agreement with the observed frequencies. However, a number of papers have since argued that this calculation uses an incorrect value for the shear modulus of the vortex

lattice [69, 24]. When the recalculated value of the shear modulus, which is an order of magnitude higher, is used, the experimental results seem to indicate that the gas is not in the LLL regime. Although in this study we mainly consider two-component BECs, our method is applicable to the single-component lattice, and our calculations are in excellent agreement with the latter value for the shear modulus, suggested by Sonin [69].

The versatility of the trapped cold atom experiments have enabled the creation of new superfluids, such as mixtures and spinor condensates. In a remarkable experiment the JILA group has been able to create a two-component BEC and study its behavior under rotation [73]. The equilibrium vortex lattice structures have been calculated by Mueller and Ho [58], and separately by Kasamatsu, Tsubota, and Ueda [44]. Experimentally, an interlaced square lattice of two-components has been observed. Furthermore, using an excitation procedure similar to the one-component case, vortex lattice oscillations have been induced in the two-component BEC, however, these excitations were found to be heavily damped and have not yielded a measurement for Tkachenko frequencies. Motivated by this experiment, in this study, we calculate the Tkachenko modes of a two-component vortex lattice, and investigate the structural phase transitions between different lattice geometries.

We consider a large two-component vortex lattice in the LLL regime. To simplify the calculations, we assume that both components have the same density and same scattering length within each component. As the scattering length between atoms from different components is varied, the vortex lattice goes through structural phase transitions, forming five different lattice geometries [58]. For all these lattice geometries, we calculate the elastic constants of the vortex lattice, and subsequently the dispersion relations for long-wavelength Tkachenko modes. Our main results are summarized below.

Unlike a single-component vortex lattice, where there is only one branch of Tkachenko modes, the two-component lattice has two branches. The situation is similar to phonon modes of a diatomic solid compared with a monoatomic solid. When the number of atoms per unit cell is doubled, so are the number of phonon

modes. In analogy with phonons, we call these branches acoustic Tkachenko modes, and optical Tkachenko modes. However, these names are not intended to imply that one branch couples more strongly to light than sound, or vice versa. As a simple picture, one may think that when an acoustic mode is excited two vortices inside the unit cell of the lattice oscillate in-phase. In other words, acoustic modes are oscillations of the "center of mass" of the unit cell, while the vortices positions with respect to the center of mass remain stationary. For an optical Tkachenko mode, vortices of different components oscillate in opposite phase, leaving the "center of mass" of each unit cell stationary. In this work, we choose our interactions such that there is symmetry under the exchange of components, which makes the above definitions of optical and acoustic unambiguous. If this symmetry is broken, as is the case with the parameters of the JILA experiment, there will still be two modes, but both of them will contain a mixture of acoustic and optical behavior.

For an incompressible superfluid such as helium, or at low rotation frequencies for BEC, Tkachenko modes in a single-component vortex lattice have linear wave-vector dependence $\omega_T \propto k$ [13]. However, when compressibility of the fluid becomes important, such as a BEC in the LLL, Tkachenko modes are quadratic in the wave-vector $\omega_T \propto k^2$ [12]. We find that a similar softening happens for the two-component vortex lattice. For an incompressible fluid, acoustic Tkachenko modes have linear long-wavelength behavior, while the optical Tkachenko modes are gapped. For a two-component BEC in the LLL, acoustic Tkachenko modes have quadratic wave-vector dependence $\omega_T^{\mathrm{ac}} \propto k^2$, while the optical modes are not gapped any more, but have linear wave-vector dependence $\omega_T^{\mathrm{op}} \propto k$.

Another important property of the Tkachenko modes of a single-component system is their isotropy. Tkachenko mode frequencies are independent of the direction of the excitation wave vector $\vec{k}$. This can be traced back to the fact that the underlying vortex lattice is triangular, and similar to acoustic waves in a triangular lattice, Tkachenko modes have isotropic behavior [51]. For two-component vortex lattices, this behavior is not expected any more, and indeed we find that when the underlying lattice has less than sixfold symmetry, both acoustic and optical Tkachenko modes are anisotropic. In all cases the anisotropy

reflects the reduced symmetry of the lattice, giving fourfold symmetric dispersion relations for the square lattice, and twofold symmetric spectra for rhombic and rectangular lattices.

Another interesting point about the two-component vortex lattices is the possibility of structural phase transitions between different lattice geometries. For a two-component BEC in the LLL there are five lattice structures and four structural phase transitions between them. Two of these are continuous, second-order transitions, while the other two are first-order transitions. In structural phase transitions of solids, second-order phase transitions are signalled by the softening of an acoustic-phonon mode, while first-order transitions are usually, but not always, accompanied by the softening of an optical-phonon mode. (A soft mode can be described as a branch of excitation that has zero frequency over a large range of wave vectors [49].) We find that a similar scenario plays out for the vortex lattices of two-component BECs, both second-order phase transitions have a soft acoustic Tkachenko mode. Of the two first-order phase transitions, one is accompanied by a soft optical Tkachenko mode, while the other does not have a direct effect on the long-wavelength Tkachenko spectrum of the system.

There are two other instabilities in the two-component BEC system. When the intercomponent attraction is stronger than the repulsion within each component, the gas is unstable towards collapse. In the opposite limit, when the intercomponent interaction is repulsive and stronger than the intracomponent repulsion we find an instability in the optical Tkachenko mode spectrum, most possibly signaling a transition to a phase separated state.

The chapter is organized as follows. In the next section, we introduce the Hamiltonian for the two-component rotating gas in the LLL, and introduce the different lattice types that are found by energy minimization. In Sec. 4.2, we outline our method of calculation for elastic coefficients, and calculate the shear modulus of a one-component condensate as an example. In Sec. 4.3, we write the coupled equations for the vortex modes and density modes, which are valid for all lattice types. In the next five sections 4.4 -4.8, we calculate the elastic energy for each lattice type, and by solving the coupled equations, we find the

dispersion relations of acoustic and optical Tkachenko modes. We also study the directional dependence of the dispersion relations and the polarization of the Tkachenko modes for each lattice type. In Sec. 4.9, we discuss the structural phase transitions and identify the soft modes associated with each transition.

4.1 Vortex lattices of two-component BEC

In this section, we consider the equilibrium vortex lattice configurations of a two-component BEC. This problem has been studied in the LLL regime analytically by Mueller and Ho [58], and for general rotation frequencies numerically by Kasamatsu *et al.* [44]. We confine ourselves to the LLL and our method of calculation of the elastic constants relies on the analytic approach developed by Mueller and Ho.

We consider a two-component BEC in a quadratic trap with trapping frequency ω. The trap frequency, the mass of the particles m, and the total number of particles are assumed to be the same for both components. We take the gas to be rotating at frequency Ω, and assume that the total number of particles in each component is large enough to form a large vortex lattice without a breakdown of the mean-field description of the system. Furthermore, we assume that the scattering lengths of the particles are such that, interaction parameters satisfy

$$\begin{aligned} g_{11} &= g_{22} = g, \\ g_{12} &= \alpha g. \end{aligned} \tag{4.1}$$

We investigate the behavior of vortex lattice geometry and the Tkachenko modes as the ratio of intercomponent scattering length to intracomponent scattering length α is varied,

$$\alpha = \frac{g_{12}}{g}. \tag{4.2}$$

We limit our discussion of vortex lattices to two dimensions, assuming that the vortex lattice is not modified along the rotation axis. This assumption is not very restrictive, as it has been shown that if the cloud is sufficiently broad in the

third dimension, vortex bending is negligible except at the edges of the cloud [40]. In the opposite limit of a two-dimensional condensate, our approach is formally valid, however, mean-field theory may not be reliable for such a system. The energy functional for our system can be written as

$$E = \sum_{i=1,2} \int d^2 r \Psi_i^*(r) \left(-\frac{\hbar^2}{2m} \nabla^2 + \frac{1}{2} m\omega^2 r^2 - \Omega L_z \right) \Psi_i(r) + V_{\text{int}}. \tag{4.3}$$

Here Ψ_i is the wave function of component i, L_z is the angular momentum along the rotation direction and V_{int} is the interaction energy given as

$$V_{\text{int}} = g \int d^2 r \left(\frac{1}{2} \left[|\Psi_1(r)|^4 + |\Psi_2(r)|^4 \right] + \alpha |\Psi_1(r)|^2 |\Psi_2(r)|^2 \right). \tag{4.4}$$

When the rotation frequency is close enough to the trapping frequency the particles can only populate levels in the LLL. For such a gas, which is in the mean-field quantum Hall regime, the wave functions have the form

$$\Psi_i(r) = f_i(z) e^{-\frac{z\bar{z}}{2\sigma^2}}, \tag{4.5}$$

where $z = x + iy$ and σ is the radius of the cloud. The requirement of analyticity on the wave function essentially determines the form of the wave function in terms of the positions of the vortices (up to an entire function with no zeros). Thus it is possible to introduce a variational wave function, using just the lattice basis vectors as variational parameters.

For a two-component BEC, when both of the components are rotating at the same frequency, vortex lattices in each component have the same lattice structure, but are shifted from each other. Thus in the LLL, we can determine the wave functions for both components in terms of just three, two-dimensional vectors $\vec{a}_1$ and $\vec{a}_2$, the basis vectors of the lattice, and $\vec{d}$, the offset between the two lattices. Thus the vortices of the first component are at $\vec{r}_{1,n,m} = n\vec{a}_1 + m\vec{a}_2$, with n, m integers, while the vortices of the second component are at $\vec{r}_{2,n,m} = n\vec{a}_1 + m\vec{a}_2 + \vec{d}$. Although we need six real numbers to describe these three vectors, the actual number of variational parameters is lower, namely 4. First of all, the vortex density ν_c^{-1} is fixed by rotation frequency Ω, thus it is possible to fix the length of one of the vectors and scale all others by this length. Second, the rotational

symmetry of the problem permits one to fix the overall orientation of the vectors. We choose the first lattice basis vector $\vec{a}_1$ to lie along the $\hat{x}$ direction, and denote its length as a_1. The remaining two vectors can then be written as

$$\begin{aligned} \vec{a}_2 &= a_1(u\hat{x} + v\hat{y}), \\ \vec{d} &= a_1[(a+bu)\hat{x} + bv\hat{y}]. \end{aligned} \tag{4.6}$$

The variational calculation is made in terms of the dimensionless parameters u, v, a, b, and then the length a_1 is fixed by requiring the wave function to have correct density of vortices $\nu_c = a_1^2 v$.

Once the positions of the vortices are known one can write the variational wave function as a Jacobi Elliptic function Θ, or as one of the doubly periodic functions that are related to the Θ up to an entire function, such as the σ function or the modified ζ function [70, 71, 72]. In terms of the Jacobi theta function we can write

$$\begin{aligned} \Psi_1(z) &= N_1\Theta(\zeta,\tau)\exp(\frac{\pi z^2}{2\nu_c} - \frac{z\bar{z}}{2l}), \\ \Psi_2(z) &= N_2\Theta(\zeta - (a+bu+ibv),\tau)\exp(\frac{\pi z^2}{2\nu_c} - \frac{z\bar{z}}{2l}). \end{aligned} \tag{4.7}$$

Here $\zeta = z/a_1$, $\tau = u + iv$, $l = \sqrt{\hbar/m\omega}$, and N_1, N_2 are normalization constants to be determined. With these wave functions we calculate the densities of the two-components as

$$\begin{aligned} |\Psi_1(\vec{r})|^2 &= Cg(\vec{r})e^{-r^2/\sigma^2}, \\ |\Psi_2(\vec{r})|^2 &= Cg(\vec{r}-\vec{d})e^{-r^2/\sigma^2}, \end{aligned} \tag{4.8}$$

where the function g is periodic with lattice vectors,

$$g(\vec{r} + n\vec{a_1} + m\vec{a_2}) = g(\vec{r}), \tag{4.9}$$

for all integers n, m. The periodic part of the density admits a Fourier series representation in terms of the reciprocal-lattice basis vectors,

$$g(\vec{r}) = \frac{1}{\nu_c}\sum_{\vec{K}} g_{\vec{K}} e^{i\vec{r}\cdot\vec{K}}, \tag{4.10}$$

with the sum carried out over all reciprocal lattice points generated by $\vec{K}_1 = \frac{2\pi}{\nu_c}\vec{a}_2 \times \hat{z}$ and $\vec{K}_2 = -\frac{2\pi}{\nu_c}\vec{a}_1 \times \hat{z}$. The utility of using the Jacobi theta function is that the Fourier components of $g_{\vec{K}}$ can be calculated with relative ease. For $\vec{K} = m_1\vec{K}_1 + m_2\vec{K}_2$ one has

$$g_{\vec{K}} = (-1)^{m_1+m_2+m_1m_2} e^{-\frac{\nu_c \vec{K}^2}{8\pi}} \sqrt{\frac{\nu_c}{2}}. \tag{4.11}$$

In the LLL, the lattice structure is entirely determined by the interaction energy. For the parameters used here minimization of the interaction energy reduces to a minimization of the following simple quantity with respect to u, v, a, and b:

$$J = \sum_{\vec{K}} \left| \frac{g_{\vec{K}}}{g_{\vec{0}}} \right|^2 \left(1 + \alpha \cos(\vec{K} \cdot \vec{d})\right). \tag{4.12}$$

It must be noted that this expression is obtained in the limit of a very large vortex lattice, formally setting the cloud radius σ to infinity. The minimization of J is done numerically with considerable ease as the Fourier coefficients of the density $g_{\vec{K}}$ are known analytically. For each value of $\alpha = g_{12}/g$, J can be calculated by truncating the rapidly converging sum to the desired accuracy, and the values u_*, v_*, a_*, b_* that minimize J can be found. These values determine the lattice geometry for each component and also the offset of the lattices of two-components.

As the ratio of the intercomponent interaction to intracomponent interaction α is varied, five different lattice types are found to minimize the interaction energy. Here, we give a brief description of each lattice, and in Secs. 4.4 - 4.8, the Tkachenko spectrum for each lattice type is calculated.

When the interaction between the two-components is attractive, i.e., $\alpha < 0$, the system minimizes its energy by positioning the vortex lattices of two-components on top of each other. However, for very large attraction, $\alpha < -1$, there is an instability towards collapse. In the range $-1 < \alpha < 0$, both components form triangular lattices which overlap with each other (See fig. 4.1). This overlapped triangular lattice is described by the parameters $u_* = 1/2, v_* = \sqrt{3}/2, a_* = b_* = 0$, which do not change with α in the given range. We find, however, that the elastic constants of the lattice depend on α, and so do the Tkachenko modes.

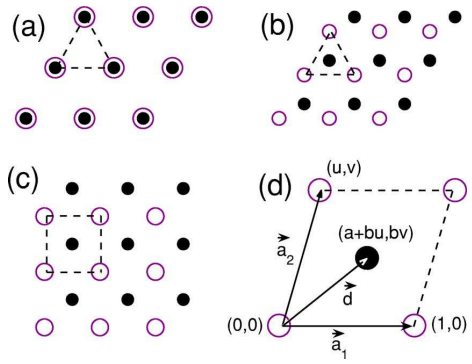

Figure 4.1: Lattice geometry for an overlapped triangular lattice (a), an interlaced triangular lattice (b), and a square lattice (c). Unit cells are shown with dashed lines. (d) Unit cell geometry for an arbitrary lattice. White and black dots represent vortices of different components. Definitions of a, b, u, v are given in Sec. 4.1.

If the intercomponent interaction becomes repulsive, it is no more favorable to put the two vortex lattices on top of each other. Instead, the most favorable places to put the vortices of one-component would be the density maxima of the other component. This simple insight holds true for all lattice types found by the minimization procedure, however the lattice type of each component changes as α is varied. For weak repulsion between the components, $0 < \alpha < 0.1724$, each component forms a triangular lattice. Within a unit cell, there is more than one density maximum, so it would seem that there are multiple positions for the vortex lattice of the second component to be placed. However, these positions are related with the overall symmetry of the lattice, so the minimization procedure gives the lattice parameters $u_* = 1/2, v_* = \sqrt{3}/2, a_* = b_* = 1/3$. Again, the overall structure of this interlaced triangular lattice (see Fig. 4.1) does not change with α. At $\alpha = 0.1724$, there is a first-order phase transition from an interlaced triangular lattice to a rhombic lattice. In the range $0.1724 < \alpha < 0.3733$, the unit cell of vortex lattices of each component are rhombuses. The vortex lattice of one-component is placed at the center of the rhombuses formed by the vortex lattice of the other component. The angle of the rhombus η (see Fig. 4.2), varies continuously from 67.9° to 90°, while the offset remains the same, $a_* = b_* = 1/2$. At $\alpha = 0.3733$, there is a second-order phase transition to a square lattice. In the range $0.3733 < \alpha < 0.9256$, the lattice is parameterized by $u_* = 0, v_* = 1, a_* = b_* = 1/2$ (see Fig. 4.2). As the interaction is increased further, there

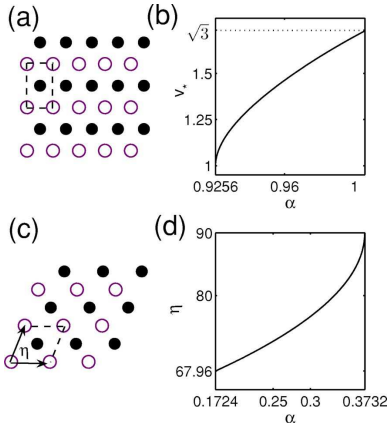

Figure 4.2: (a) Lattice geometry for a rectangular lattice; a unit cell is shown with dashed lines. (b) Change of the aspect ratio of the rectangle v_* with respect to interaction strength α. The unit cell grows in the y direction as $\alpha \to 1$. At $\alpha = 1$, $v_* = \sqrt{3}$. (c) Lattice geometry of a rhombic lattice, dashed lines showing a unit cell. η is twice the opening angle of the rhombic unit cell. (d) Plot of η vs α for the rhombic lattice. As $\alpha \to 0.3732$, $\eta \to 90°$, and the rhombus continuously changes to a square. At $\alpha = 0.1724$, η makes a jump from 60° to 67.958°.

is a second-order phase transition to a rectangular lattice at $\alpha = 0.9256$. In a rectangular lattice, vortices of one-component are always found at the centers of the rectangles formed by the vortices of the other component, i.e., $a_* = b_* = 1/2$. However, the aspect ratio of the rectangle increases continuously.

For a nonrotating system, there is a phase-separation instability at $\alpha = 1$. This instability is not found in the results of the energy minimization described above. However, when the coupling between the density oscillations and vortex motion is taken into account, as in Sec. 4.7, it is found that at this point there is an instability. Thus the system is not described by a vortex lattice beyond $\alpha = 1$.

After a survey of the possible lattice structures and the analytic method that is used to find these structures, in the next section we describe how the same analytic approach can be used to calculate the elastic constants of the discussed vortex lattices.

4.2 Numerical calculation of elastic constants

The power of the analytic approach introduced in the previous section is that it can also be used to calculate the energies of lattice structures which are slightly deformed from the minimum-energy configuration. As the numerical calculation of the energy for a given lattice is quite simple, it is possible to evaluate the energy for configurations where lattice parameters have small deviations from their minimum-energy values. Such small deviations can also be described by a hydrodynamic approach. Assuming that the lattice deformations are sufficiently smooth, the vortex lattice can be treated as an elastic medium. The form of the elastic energy is constrained by symmetries of the lattice, and for small deformations, can always be taken as quadratic in displacements. Thus the long-wavelength behavior of the lattice is described by an elastic energy that is quadratic in the vortex displacement field, and the problem reduces to the calculation of the elastic constants, which are the coefficients of the quadratic terms in vortex displacements.

Our approach is to numerically calculate the energy of the vortex lattice close to the equilibrium position, and then find the elastic coefficients of the vortex lattice by making quadratic fits to the calculated energy. As a demonstration of this method, we first calculate the shear modulus of the triangular lattice of a one-component BEC. A vortex lattice in a one-component BEC is parameterized by two two-dimensional vectors $\vec{a}_1, \vec{a}_2$, the lattice basis vectors. The lattice basis vectors define the equilibrium positions of the vortices, and we denote the deviation of the vortex at lattice site n, m, from its equilibrium by the vector $\vec{\epsilon}_{n,m}$. So the position of the vortex $\vec{r}_{n,m}$ is

$$\vec{r}_{n,m} = n\vec{a}_1 + m\vec{a}_2 + \vec{\epsilon}_{n,m}. \tag{4.13}$$

If the vortex displacements are sufficiently smooth over large length scales, one can describe a long-wavelength vortex displacement field $\vec{\epsilon}(x, y) = \epsilon_x(x, y)\hat{x} + \epsilon_y(x, y)\hat{y}$ by a suitable coarse-graining procedure. For a triangular lattice, the elastic energy density can then be written as

$$\varepsilon_{\text{elastic}} = C_1 \left(\frac{\partial \epsilon_x}{\partial x} + \frac{\partial \epsilon_y}{\partial y} \right)^2 + C_2 \left[\left(\frac{\partial \epsilon_x}{\partial x} - \frac{\partial \epsilon_y}{\partial y} \right)^2 + \left(\frac{\partial \epsilon_x}{\partial y} + \frac{\partial \epsilon_y}{\partial x} \right)^2 \right]. \tag{4.14}$$

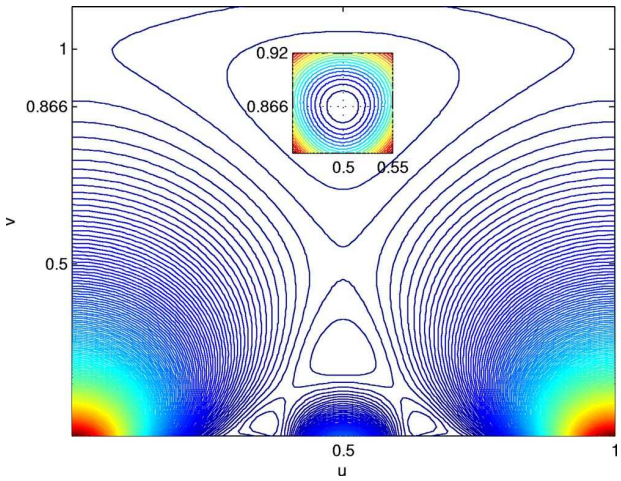

Figure 4.3: Contour plot of the energy for a one-component triangular lattice, Eq. (4.15). The inset is a closer view around the equilibrium point. Circular contours indicate that quadratic fit of Eq. (4.16) is possible.

For a gas in the LLL, compression modulus is zero, $C_1 = 0$ [13]. Using the analytic method introduced above, the shear modulus C_2 is determined as follows.

For a one-component vortex lattice, the minimum-energy configuration is found by minimizing

$$I = \sum_{\vec{K}} \left| \frac{g_{\vec{K}}}{g_{\vec{0}}} \right|^2 , \tag{4.15}$$

and yields $u_* = 1/2, v_* = \sqrt{3}/2$, the triangular lattice. We calculate the energy around this point by varying u and v from their equilibrium values. A contour plot of the energy around the equilibrium point is given in Fig. 4.3. To this form we can successfully fit a quadratic form, giving us an elastic energy of the form

$$E_{\text{elastic}} = \frac{gn^2}{2} \left[C_u (u - u_*)^2 + C_v (v - v_*)^2 + C_{uv} (u - u_*)(v - v_*) \right] , \tag{4.16}$$

and determine

$$\begin{aligned} C_u &= 0.3177, \\ C_v &= 0.3177, \\ C_{uv} &= 0.000. \end{aligned} \tag{4.17}$$

The fact that $C_u = C_v$ shows that there is only one shear modulus for a triangular lattice, and validates our numerical procedure. To find the connection

between C_u and the shear modulus C_2, we must determine the displacement field corresponding to small changes of the lattice basis vectors. By taking into account that the unit-cell volume is fixed by rotational frequency, the correspondence between u, v and vortex displacement field is found as

$$\begin{aligned} \frac{\partial \epsilon_x}{\partial y} &= \frac{u-u_*}{v_*}, \qquad \frac{\partial \epsilon_x}{\partial x} = -\frac{v-v_*}{2v_*}, \\ \frac{\partial \epsilon_x}{\partial y} &= \frac{v-v_*}{2v_*}, \qquad \frac{\partial \epsilon_x}{\partial y} = 0. \end{aligned} \tag{4.18}$$

By substituting these expressions in Eq. (4.14), using $u_* = 1/2, v_* = \sqrt{3}/2$ and comparing with Eq. (4.16) we obtain

$$C_2 = \frac{3}{8} C_u = 0.1191 g n^2. \tag{4.19}$$

This value is an order of magnitude larger than the value used by Baym [12], and is in excellent agreement with Sonin [69]. This is not surprising, as our method of obtaining the shear modulus is equivalent to the deformation of the lattice used by Sonin. However, the simplicity of our numerical method enables us to calculate the elastic coefficients of more complex lattices, such as the two-component lattices discussed in this study.

For a two-component lattice, the energy of the lattice depends not only on the lattice basis vectors, but also on the offset of two lattices from each other. Hence there are four variational parameters u, v, a, b. Elastic energy around the minimum-energy point has to be expressed as a quadratic form in all of these variables. We numerically calculate the energy of the lattice for many points around the minimum-energy point and then express the elastic energy by fitting to a form

$$\begin{aligned} E_{\text{elastic}} = \frac{gn^2}{2} [&C_u (u-u_*)^2 + C_v (v-v_*)^2 + C_{uv} (u-u_*)(v-v_*) + \\ &C_a (a-a_*)^2 + C_b (b-b_*)^2 + C_{ab} (a-a_*)(b-b_*)]. \end{aligned}$$

Here, due to the symmetry between component 1 and component 2, it is not necessary to include terms that mix displacements a, b with deformations of the lattice u, v. This is essentially the decoupling of optical Tkachenko modes from acoustic Tkachenko modes as discussed in Sec. 1.

In the next section, we give the hydrodynamic equations for a two-component condensate, but leave the form of the elastic energy unspecified. In the following sections, the form of the elastic energy and the values of the elastic constants are given separately for each lattice type. After the elastic energy is specified, hydrodynamic equations are solved and the dispersion relations for Tkachenko modes are obtained.

4.3 Hydrodynamic equations

The oscillations of vortices about their equilibrium positions can be described by a hydrodynamic theory by treating the vortex lattice as an elastic medium. For trapped BECs it is important to take into account the compressibility of the gas, as the vortex lattice oscillations are coupled to density oscillations in a nontrivial way. The superfluid hydrodynamics that takes this effect into account has been developed by a number of groups in the context of superfluid He [13], and more recently applied to rotating BECs by Baym [12]. Here we describe the hydrodynamics of a two-component vortex lattice by generalizing this hydrodynamics to a two-component BEC.

As the hydrodynamic variables, we use the densities of each component $n_i(\vec{r},t)$, corresponding velocity fields $\vec{v}_i(\vec{r},t)$, and the vortex displacement fields $\vec{\epsilon}_i(\vec{r},t)$ introduced in the previous section. Here $i = 1,2$ is component index, giving us a total of six hydrodynamic fields. However, not all of these fields are independent, as is apparent in the calculation below. We also set $\hbar = 1$ in the calculation for convenience.

The long-wavelength average of the velocity field is not irrotational, but is linked to the compressions of the vortex lattice,

$$\vec{\nabla} \times \vec{v}_i = -2\Omega\vec{\nabla} \cdot \vec{\epsilon}_i, \qquad i = 1,2. \tag{4.20}$$

Similarly the superfluid acceleration equation holds for each component

$$m\left(\frac{\partial \vec{v}_i}{\partial t} + 2\vec{\Omega} \times \frac{\partial \vec{\epsilon}_i}{\partial t}\right) = -\vec{\nabla}\mu_i, \qquad i = 1,2. \tag{4.21}$$

Here μ_i is the chemical potential of component i. Below we leave the index i unspecified to indicate that the equation is valid for both components.

The conservation of particle number results in the continuity equation

$$\frac{\partial n_i}{\partial t} + \vec{\nabla} \cdot (n_i \vec{v}_i) = 0, \tag{4.22}$$

while momentum conservation gives

$$m\left(n_i \frac{\partial \vec{v}_i}{\partial t} + 2n_i \vec{\Omega} \times \vec{v}_i\right) + \vec{\nabla} P_i = -\vec{\sigma}_i. \tag{4.23}$$

Here P_i is the pressure, related to the chemical potential as $\vec{\nabla} P_i = n_i \vec{\nabla} \mu_i$, and for a weakly interacting two-component condensate satisfies

$$\begin{aligned} \vec{\nabla} P_1 &= gn\vec{\nabla} n_1 + \alpha gn \vec{\nabla} n_2, \\ \vec{\nabla} P_2 &= gn\vec{\nabla} n_2 + \alpha gn \vec{\nabla} n_1. \end{aligned} \tag{4.24}$$

The stress vectors σ_i are obtained by taking the functional derivative of the elastic energy with respect to vortex displacement fields, as in elasticity theory,

$$\vec{\sigma}_i = \frac{\delta E_{\text{elastic}}}{\delta \vec{\epsilon}_i}. \tag{4.25}$$

Using Eqs. (4.23) and (4.20), we have

$$2m\vec{\Omega} \times \left(\frac{\partial \vec{\epsilon}_i}{\partial t} - \vec{v}_i\right) = \frac{\vec{\sigma}_i}{n}. \tag{4.26}$$

The curl and divergence of these equations lead to

$$\vec{\nabla} \cdot \left(\frac{\partial \vec{\epsilon}_i}{\partial t} - \vec{v}_i\right) = \frac{\vec{\nabla} \times \vec{\sigma}_i}{2\Omega nm}, \tag{4.27}$$

and

$$\vec{\nabla} \times \frac{\partial \vec{\epsilon}}{\partial t} + 2\Omega \vec{\nabla} \cdot \vec{\epsilon}_i = -\frac{\vec{\nabla} \cdot \vec{\sigma}_i}{2\Omega nm}. \tag{4.28}$$

Similarly, the divergence of the superfluid acceleration equation gives

$$\begin{aligned} \left(-\frac{\partial^2}{\partial t^2} + \frac{gn}{m}\nabla^2\right) n_1 + \alpha \frac{gn}{m} \nabla^2 n_2 &= 2\Omega n \vec{\nabla} \times \frac{\partial \vec{\epsilon_1}}{\partial t}, \\ \left(-\frac{\partial^2}{\partial t^2} + \frac{gn}{m}\nabla^2\right) n_2 + \alpha \frac{gn}{m} \nabla^2 n_1 &= 2\Omega n \vec{\nabla} \times \frac{\partial \vec{\epsilon_2}}{\partial t}. \end{aligned} \tag{4.29}$$

At this stage it is preferable to take advantage of the symmetry of the equations under the exchange of component 1 with component 2. We define the symmetric and antisymmetric variables as

$$\begin{aligned} n_+ &= n_1 + n_2, \qquad \vec{\epsilon}_+ = \vec{\epsilon}_1 + \vec{\epsilon}_2, \qquad \vec{\sigma}_+ = \vec{\sigma}_1 + \vec{\sigma}_2, \\ n_- &= n_1 - n_2, \qquad \vec{\epsilon}_- = \vec{\epsilon}_1 - \vec{\epsilon}_2, \qquad \vec{\sigma}_- = \vec{\sigma}_1 - \vec{\sigma}_2. \end{aligned} \tag{4.30}$$

In terms of these variables we obtain two sets of three equations, where each set is decoupled from the other. The polarization of the Tkachenko modes are controlled by the polarization equation

$$\vec{\nabla} \times \frac{\partial \vec{\epsilon}_\pm}{\partial t} + 2\Omega \vec{\nabla} \cdot \vec{\epsilon}_\pm = -\frac{1}{2mn\Omega} \vec{\nabla} \cdot \vec{\sigma}_\pm. \tag{4.31}$$

The usual sound mode equations for a two-component fluid are modified by the dynamics of the vortex lattice as

$$-\frac{\partial^2 n_\pm}{\partial t^2} + (1 \pm \alpha) \frac{gn}{m} \nabla^2 n_\pm = 2n\Omega \vec{\nabla} \times \frac{\partial \vec{\epsilon}_\pm}{\partial t}. \tag{4.32}$$

The dynamics of the vortex lattice and its interaction with the density modes is governed by

$$\vec{\nabla} \cdot \frac{\partial^2 \vec{\epsilon}_\pm}{\partial t^2} + \frac{1}{n} \frac{\partial^2 n_\pm}{\partial t^2} = \frac{1}{2nm\Omega} \frac{\partial}{\partial t} \vec{\nabla} \times \vec{\sigma}_\pm. \tag{4.33}$$

Equations (4.31)-(4.33) form a linear set of six equations. However, as the stresses $\sigma_\pm$, depend only on the lattice displacements $\epsilon_\pm$, with the same sign, the three symmetric variable (+) equations are decoupled from the antisymmetric variable (−) equations. Thus the "+" set describes the acoustic Tkachenko modes and their coupling with the "in-phase" sound mode, while the "−" set describes the optical Tkachenko modes and their coupling to the "out-of-phase" sound mode.

In the following sections, we specify the elastic energy E_{elastic} for each lattice type, and calculate the dispersion relations of both acoustic and optical Tkachenko modes. Each section starts with a brief description of the properties of the lattice type under consideration. Subsequently we give the form of the elastic energy for this lattice type and the values of the numerically calculated elastic constants. We then outline the solutions of the Tkachenko mode equations Eqs. (4.31)-(4.33), for the specific form of the elastic energy, and derive the dispersion relations of the acoustic and optical modes. Each section is concluded by a discussion of the properties of the dispersion relation.

4.4 Overlapped triangular lattice

When the interaction between the two-components is attractive, it is energetically preferable to have the density minima of the two-components to coincide. However, if the intercomponent attraction is too strong there will be a collapse type instability. This insight is validated by the calculations mentioned in Sec. 4.1, where for $-1 < \alpha < 0$, the equilibrium lattice structure is triangular for both components and the vortex lattices of the two-components coincide. This overlapped triangular lattice is described by

$$u_* = 1/2, \qquad v_* = \sqrt{3}/2, \qquad a_* = b_* = 0. \tag{4.34}$$

The elastic energy in all the vortex lattices can be separated into two parts, elastic energy due to acoustic displacements ϵ_+, and elastic energy due to optical displacements ϵ_-. There will not be any terms that contain both, as such contributions to energy change sign under the exchange of components. So we can write

$$E_{\text{elastic}} = E^{\text{ac}}_{\text{elastic}} + E^{\text{op}}_{\text{elastic}}. \tag{4.35}$$

The acoustic contribution to the elastic energy will have the same form that is valid for a triangular lattice. In the LLL the hydrostatic compression modulus is zero and we need to consider only the shear modulus,

$$E^{\text{ac}}_{\text{elastic}} = \int d^2 r C^{\text{ac}} \left[\left(\frac{\partial \epsilon^x_+}{\partial x} - \frac{\partial \epsilon^y_+}{\partial y} \right)^2 + \left(\frac{\partial \epsilon^x_+}{\partial y} + \frac{\partial \epsilon^y_+}{\partial x} \right)^2 \right]. \tag{4.36}$$

Similarly, the only quadratic form one can make from ϵ_- which does not break the sixfold symmetry of the lattice is

$$E^{\text{op}}_{\text{elastic}} = \int d^2 r C^{\text{op}} \left(\vec{\epsilon}_- \right)^2. \tag{4.37}$$

The two elastic constants, C^{ac} and C^{op}, control the acoustic and optical Tkachenko modes, respectively. These two constants, however, have different dimensions, as is clear from their definition. We first nondimensionalize these constants as follows.

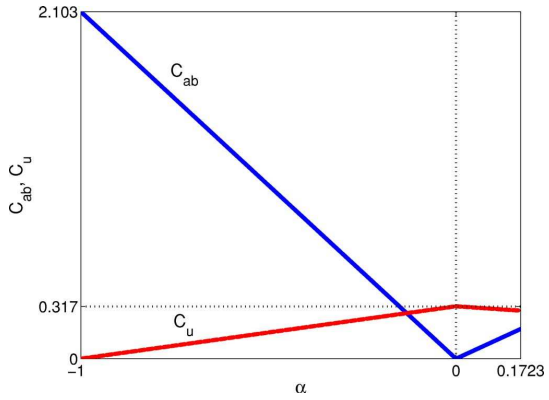

Figure 4.4: Elastic constants (C_{ab}, C_u) of overlapped $(-1 < \alpha < 0)$ and interlaced $(0 < \alpha < 0.1723)$ triangular lattices with respect to α. As the attraction between the components increases $(\alpha \to -1)$, C_{ab} increases, and C_u decreases linearly. When there is no interaction between components $(\alpha = 0)$, $C_{ab} = 0$ which causes the discontinuity in the transition to interlaced triangular lattice. At $\alpha = 0$, the value of C_u is equal to the shear modulus of a one-component vortex lattice.

For the acoustic shear modulus, we can define a dimensionless quantity $\tilde{C}^{\rm ac}$,

$$\tilde{C}^{\rm ac} = \frac{C^{\rm ac}}{gn^2}. \tag{4.38}$$

As explained in Sec. 4.2, we can fit the energy near the minimum to a quadratic form,

$$E^{\rm ac}_{\rm elastic} = \frac{1}{2} gn^2 C_u \left[(u - u^*)^2 + (v - v_*)^2 \right], \tag{4.39}$$

which yields for the triangular lattice with $v_* = \sqrt{3}/2$

$$\tilde{C}^{\rm ac} = \frac{3}{8} C_u. \tag{4.40}$$

The results of numerical calculation for C_u are displayed in Fig. 4.4. At $\alpha = 0$, the shear modulus for the acoustic modes takes the single-component value (per component) as expected from two noninteracting vortex lattices. As α is decreased towards -1, the shear modulus decreases linearly, signalling the collapse instability expected due to attractive interaction between the components.

Similarly the optical elastic constant can be nondimensionalized as

$$\tilde{C}^{\rm op} = \frac{d^2}{gn^2} C^{\rm op}, \tag{4.41}$$

where d is the lattice constant for the triangular lattice, which is related to rotation frequency as

$$d^2 = \frac{2\pi}{\sqrt{3}m\Omega}. \tag{4.42}$$

The optical part of the elastic energy can be fitted to the rotationally invariant form

$$E^{\rm op}_{\rm elastic} = \frac{gn^2}{2} C_{ab}[(a-a_*) + u_*(b-b_*)]^2 + [v_*(b-b_*)]^2. \tag{4.43}$$

which results in

$$\tilde{C}^{\rm op} = \frac{1}{2} C_{ab}. \tag{4.44}$$

The result of numerical calculation for C_{ab} is plotted in Fig. 4.4. As α is decreased towards -1, it gets harder to separate the vortices of two-components, as expected from the increasing attraction between the components.

Once the elastic constants are known, the calculation of the Tkachenko modes for different lattices are straightforward, albeit tedious. In this section, we give a detailed calculation, while for all other lattice types we simply present the results of the calculation.

We first start with the calculation of the acoustic Tkachenko modes. With the form of the elastic energy given above, the acoustic stress is

$$\vec{\sigma}_+ = -4C^{\rm ac}\nabla^2\vec{\epsilon}_+. \tag{4.45}$$

Fourier transforming, we get $\vec{\sigma}_+ = 4C^{\rm ac}k^2\vec{\epsilon}_+$. Now, we also Fourier transform the polarization equation (4.31) to obtain

$$\epsilon^y_+ = \frac{N_1}{D_1}\epsilon^x_+, \tag{4.46}$$

with

$$\begin{aligned} N_1 &= -i\omega k_y - 2\Omega k_x - \frac{2C^{\rm ac}}{mn\Omega}k^2 k_x, \\ D_1 &= -i\omega k_x + 2\Omega k_y + \frac{2C^{\rm ac}}{mn\Omega}k^2 k_y. \end{aligned} \tag{4.47}$$

Substituting the above result into Fourier transforms of Eqs. (4.32) and (4.33), we obtain

$$\left(\omega^2 - (1+\alpha)\frac{gn}{m}k^2\right) n_+ + n\left(4\Omega^2 + \frac{4C^{\rm ac}}{nm}k^2\right)\frac{\omega k^2}{D_1}\epsilon^x_+ = 0 \tag{4.48}$$

and

$$-\frac{\omega^2}{n}n_+ + \left(\frac{4C^{\rm ac}}{nm}k^2 - \omega^2\right)\frac{\omega k^2}{D_1}\epsilon_+^x = 0. \tag{4.49}$$

By scaling the wave vector in frequency units,

$$k' = \sqrt{\frac{gn}{m}}k, \tag{4.50}$$

and using dimensionless elastic constants we obtain the characteristic equation as

$$\omega^4 - \omega^2\left[4\Omega^2 + (1+\alpha+8\tilde{C}^{\rm ac})k'^2\right] + (1+\alpha)4\tilde{C}^{\rm ac}k'^4 = 0. \tag{4.51}$$

This equation describes two different modes, one is a gapped sound mode, also called the inertial mode, while the other is the acoustic Tkachenko mode of the triangular lattice. To the lowest order in the long-wavelength approximation we get

$$\begin{aligned}\omega_I^{\rm ac} &= 2\Omega + \frac{1+\alpha+8\tilde{C}^{\rm ac}}{4\Omega}k'^2, \\ \omega_T^{\rm ac} &= \sqrt{(1+\alpha)\tilde{C}^{\rm ac}}\frac{k'^2}{\Omega}.\end{aligned} \tag{4.52}$$

The inertial mode is gapped, starting at 2Ω, and the second mode is the acoustic Tkachenko mode which has quadratic dispersion at long-wavelengths, similar to the Tkachenko mode in a one-component vortex lattice.

Calculation of the optical Tkachenko mode, similarly, starts by evaluating the optical part of the stress as

$$\vec{\sigma}_- = 4C^{\rm op}\vec{\epsilon}_-. \tag{4.53}$$

From the polarization equation we get

$$\epsilon_-^y = \frac{N_1}{D_1}\epsilon_-^x, \tag{4.54}$$

with

$$\begin{aligned}N_1 &= \omega k_y - i\left(2\Omega + \frac{2C^{\rm op}}{mn\Omega}\right)k_x \\ D_1 &= \omega k_x + i\left(2\Omega + \frac{2C^{\rm op}}{mn\Omega}\right)k_y\end{aligned} \tag{4.55}$$

which results in two coupled equations obtained from Eqs. (4.32) and (4.33)

$$\left(\omega^2 - (1-\alpha)\frac{gn}{m}k^2\right)n_- + n\left(4\Omega^2 + \frac{4C^{\rm op}}{mn}\right)i\frac{\omega k^2}{D_1}\epsilon_-^x = 0, \tag{4.56}$$

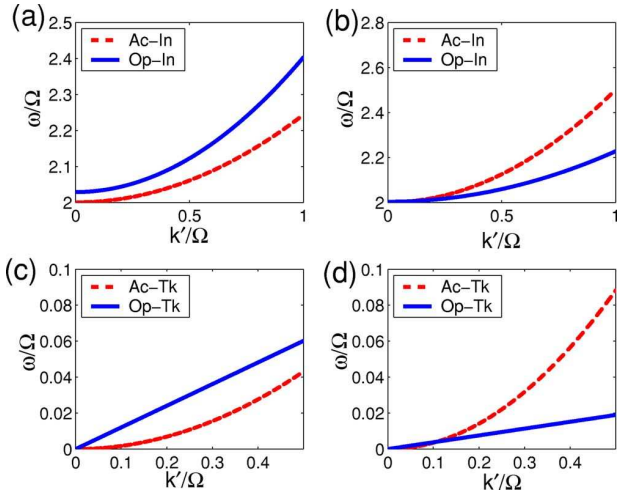

Figure 4.5: Spectrum for overlapped triangular lattice, (a), (c), at $\alpha = -0.5$, and interlaced triangular lattice (b), (d) at $\alpha = 0.1$. k' and ω are scaled to rotation frequency Ω, and $\frac{gn}{\Omega} = 0.1$. Dispersion relations are the same for both lattice types, Eqs. (4.52) and (4.58). However, the elastic constants are different (see Fig. 4.4). Both acoustic and optical inertial modes, (a), (b), are gapped. For both lattices optical Tkachenko modes are linear while acoustic Tkachenko modes are quadratic in k.

and

$$\frac{\omega^2}{n} n_- + \left[\omega^2 - \frac{2C^{\rm op}}{\Omega nm}\left(2\Omega + \frac{2C^{\rm op}}{\Omega nm}\right)\right] i\frac{\omega k^2}{D_1}\epsilon_-^x = 0. \tag{4.57}$$

Once again, using $k' = \sqrt{\frac{gn}{m}}k$, and the dimensionless elastic constants we obtain the dispersion relation for two modes,

$$\begin{aligned} \omega_I^{\rm op} &= 2\Omega\sqrt{1 + \frac{\sqrt{3}}{\pi}\tilde{C}^{\rm op}\frac{gn}{\Omega}} + \frac{1-\alpha}{4\Omega}k'^2, \\ \omega_T^{\rm op} &= \sqrt{\frac{\sqrt{3}}{2\pi}\tilde{C}^{\rm op}\frac{gn}{\Omega}}\, k'. \end{aligned} \tag{4.58}$$

These results are obtained to the lowest nonvanishing order in k' and also to the lowest order in $\frac{gn}{\Omega}$, which is a small parameter in the LLL regime.

The typical spectrum of the Tkachenko modes and the gapped sound modes are displayed in Fig. 4.5. The following properties of Tkachenko modes are revealed as a result of the above calculation.

First, we see that doubling the number of components in the BEC results in

a doubling of the modes. Because the vortex lattice oscillations are coupled to density oscillations in a compressible fluid, there are four branches of excitation. The two inertial modes correspond to in-phase and out-of-phase oscillations of the densities of two-components and are gapped, starting essentially at twice the rotation frequency. As a second point, we find that the acoustic Tkachenko mode has quadratic k dependence at long-wavelength while the optical Tkachenko mode goes linearly with k. In an incompressible fluid, we would expect to find the acoustic modes with linear dispersion and the optical modes to be gapped. This result can be obtained by explicitly decoupling the density in the above calculation. Thus the extra factor of k in the dispersion is a result of the coupling between the density and the vortex lattice oscillations.

While these two properties apply to all the lattice types considered below, there are some properties that are specific to the overlapped triangular lattice discussed in this section. First of all, the dispersion relation for both the optical and the acoustic Tkachenko modes are isotropic, i.e., independent of the direction of $\vec{k}$. The isotropy of the excitations is a direct consequence of the sixfold symmetry of the underlying lattice. The elastic (sound) waves in a triangular lattice also show isotropic behavior [51] and as we view the Tkachenko modes as the elastic excitations of the vortex lattice, this result is not unexpected. However, for the other, nontriangular, lattice types considered below, Tkachenko mode spectrum is anisotropic. A second property is revealed by investigating the behavior of the modes for changing α. As α goes to zero, the optical Tkachenko mode becomes softer and softer, revealing that the two lattices become mostly independent. Indeed at $\alpha = 0$ there is a first-order phase transition to the interlaced triangular lattice. As α approaches -1, this time it is the acoustic mode that becomes soft, and there is an instability towards collapse at exactly $\alpha = -1$. It is interesting to note that although our approach cannot describe this collapse, its signature is still present in the Tkachenko mode spectrum.

4.5 Interlaced triangular lattice

For a single-component vortex lattice the equilibrium configuration is always the triangular lattice. When the interaction between the components of a two-component vortex lattice is weak, both vortex lattices stay triangular. The offset between the two-components is, however, decided by the sign of the intercomponent interaction. For attractive interaction $\alpha < 0$, the resulting lattice is the overlapped triangular lattice discussed in the previous section. For weak and repulsive interaction, it is energetically favorable to place the vortices of one-component at the density maxima of the other component. The resulting, interlaced triangular lattice is described by

$$u_* = \frac{1}{2}, \qquad v_* = \frac{\sqrt{3}}{2}, \qquad a_* = b_* = \frac{1}{3}. \tag{4.59}$$

The interlaced triangular lattice is the minimum-energy configuration for $0 < \alpha < 0.1724$, and is displayed in Fig. 4.1.

The elastic energy and the Tkachenko mode equations follow directly from the symmetry of the lattice. As the interlaced triangular lattice has exactly the same symmetry as the overlapped triangular lattice discussed in the previous section, the calculation given in the previous section is valid also for the interlaced triangular lattice. It is only the values of the elastic constants $\tilde{C}^{\rm ac}$ and $\tilde{C}^{\rm op}$, and their dependence on α, that is different from the previous case.

As a result, the acoustic modes are given by

$$\begin{aligned} \omega_I^{\rm ac} &= 2\Omega + \frac{1+\alpha+8\tilde{C}^{\rm ac}}{4\Omega} k'^2, \\ \omega_T^{\rm ac} &= \sqrt{(1+\alpha)\tilde{C}^{\rm ac}} \frac{k'^2}{\Omega} \end{aligned} \tag{4.60}$$

and the optical modes are given by

$$\begin{aligned} \omega_I^{\rm op} &= 2\Omega \sqrt{1 + \frac{\sqrt{3}}{\pi}\tilde{C}^{\rm op}\frac{gn}{\Omega}} + \frac{1-\alpha}{4\Omega} k'^2, \\ \omega_T^{\rm op} &= \sqrt{\frac{\sqrt{3}}{2\pi}\tilde{C}^{\rm op}\frac{gn}{\Omega}}\, k'. \end{aligned} \tag{4.61}$$

Here the relations between $C^{\rm op}, C^{\rm ac}$ and C_u, C_{ab}, remain the same as in the previous section. A plot of the elastic constants is given in Fig. 4.4.

As in the previous section, we see that the acoustic Tkachenko mode is quadratic in k, at long-wavelengths, while the optical Tkachenko mode is linear in k. As a consequence of the sixfold symmetry of the underlying lattice, both modes are isotropic. A typical spectrum of the Tkachenko modes is displayed in Fig. 4.5. Just as the optical Tkachenko mode becomes soft for the overlapped triangular lattice as $\alpha = 0$ is approached from below, a similar softening takes place for the interlaced triangular lattice. So both sides of the first-order transition have dynamics characterized by a soft optical mode.

4.6 Square lattice

The lattice type which is energetically favorable over the largest range of intercomponent interaction is the square lattice. For $0.3733 < \alpha < 0.9256$, one-component's vortex lattice forms a square lattice while the other components vortices are situated at the centers of the squares (see Fig. 4.1). This lattice is characterized by

$$u_* = 0, \qquad v_* = 1, \qquad a_* = b_* = \frac{1}{2}. \tag{4.62}$$

For the square lattice we can write the elastic energy due to optical and acoustic deformations as

$$E_{\rm elastic} = E^{\rm ac}_{\rm elastic} + E^{\rm op}_{\rm elastic} \tag{4.63}$$

with

$$\begin{aligned} E^{\rm ac}_{\rm elastic} &= \frac{1}{2}\int d^2r \left[C_1^{\rm ac} \frac{\partial \epsilon_+^x}{\partial x}\frac{\partial \epsilon_+^y}{\partial y} + C_2^{\rm ac}\left(\frac{\partial \epsilon_+^x}{\partial y} + \frac{\partial \epsilon_+^y}{\partial x}\right)^2\right], \qquad (4.64)\\ E^{\rm op}_{\rm elastic} &= \int d^2r C^{\rm op}\left(\vec{\epsilon}_-\right)^2. \end{aligned}$$

For acoustic modes we define the dimensionless elastic constants

$$\tilde{C}_1^{\rm ac} = \frac{C_1^{\rm ac}}{gn^2}, \qquad \tilde{C}_2^{\rm ac} = \frac{C_2^{\rm ac}}{gn^2}, \tag{4.65}$$

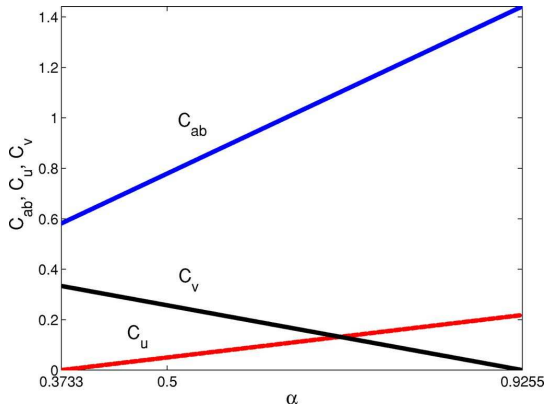

Figure 4.6: Elastic constants (C_{ab}, C_u, C_v) of square lattice, Eqs. (4.66) and (4.74). As the components attract each other more, C_{ab} increases linearly. Both limits of α lead to second-order phase transitions. C_u and C_v vanish at $\alpha = 0.3733$ and $\alpha = 0.9255$, respectively.

and fit the acoustic part of the elastic energy to the form

$$E^{\rm ac}_{\rm elastic} = \frac{gn^2}{2}\left[C_u(u-u_*)^2 + C_v(v-v_*)^2\right], \tag{4.66}$$

which yield

$$\tilde{C}^{\rm ac}_1 = -4C_v, \qquad \tilde{C}^{\rm ac}_2 = C_u. \tag{4.67}$$

The variation of elastic constants C_u and C_v are plotted in Fig. 4.6.

The calculation of acoustic Tkachenko mode frequencies proceed similar to the previous sections. However, for the square lattice, the equations are not isotropic, for example the polarization equation (4.31) gives

$$\epsilon^y_+ = \frac{N_1}{D_1}\epsilon^x_+, \tag{4.68}$$

with

$$\begin{aligned} N_1 &= \left(-i\omega k_y - 2\Omega k_x - \frac{4C^{\rm ac}_2 + C^{\rm ac}_1}{2nm\Omega}k_x k_y^2\right), \\ D_1 &= \left(-i\omega k_x + 2\Omega k_y + \frac{4C^{\rm ac}_2 + C^{\rm ac}_1}{2nm\Omega}k_y k_x^2\right). \end{aligned} \tag{4.69}$$

We find, in the long-wavelength limit, the inertial mode frequency

$$\omega^{\rm ac}_I = 2\Omega + \frac{1+\alpha+2\tilde{C}^{\rm ac}_2}{4\Omega}k'^2, \tag{4.70}$$

and the acoustic Tkachenko mode frequency

$$\omega_T^{\rm ac} = \sqrt{\frac{1+\alpha}{2}}\sqrt{\left[\tilde{C}_2^{\rm ac} f_2(\theta) - \tilde{C}_1^{\rm ac} f_1(\theta)\right]})\frac{k'^2}{\Omega}. \tag{4.71}$$

Here, we have

$$f_1(\theta) = \frac{1}{4}\sin^2(2\theta), \qquad f_2(\theta) = \cos^2(2\theta), \tag{4.72}$$

where θ is the angle from the $\hat{x}$ direction when the basis vectors of the vortex lattice are taken along $\hat{x}$ and $\hat{y}$.

For the optical spectrum, we define the dimensionless elastic constant

$$\tilde{C}^{\rm op} = \frac{d^2}{gn^2} C^{\rm op}, \tag{4.73}$$

where the lattice constant d is given by $d^2 = \frac{\pi}{\Omega m}$. The optical part of the elastic energy can be numerically fitted to a form

$$E_{\rm elastic}^{\rm op} = \frac{gn^2}{2} C_{ab}\left[(a-a_*)^2 + (b-b_*)^2\right], \tag{4.74}$$

which yields

$$\tilde{C}^{\rm op} = \frac{C_{ab}}{2}. \tag{4.75}$$

The dependence of the elastic constant C_{ab} on α is plotted in Fig. 4.6.

The gapped inertial mode and the optical Tkachenko mode are calculated to the lowest order in k' and $\frac{gn}{\Omega}$ as

$$(\omega_I^{\rm op})^2 = 4\Omega^2\left[1 + \frac{2gn}{\pi\Omega}\tilde{C}^{\rm op}\right] + (1-\alpha)k'^2, \tag{4.76}$$

and

$$\omega_T^{\rm op} = \sqrt{\frac{1-\alpha}{\pi + 2\frac{gn}{\Omega}\tilde{C}^{\rm op}}}\sqrt{\frac{gn}{\Omega}\tilde{C}^{\rm op}}\, k', \tag{4.77}$$

respectively.

The above results reveal a number of properties of the Tkachenko modes of a square vortex lattice. Similar to the triangular lattice, there are two gapped modes, which are the sound modes of the two-component condensate modified by the interactions with the vortex oscillations. The remaining two gapless modes

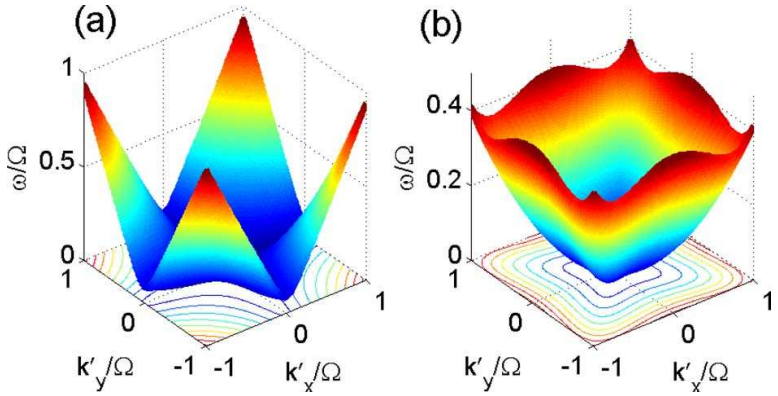

Figure 4.7: Dispersion relation of the acoustic Tkachenko modes for the square lattice, Eq. (4.71) for $\alpha = 0.4$ (a), and $\alpha = 0.85$ (b). Underlying contour plots are given to illustrate the anisotropy of the modes.

are the acoustic Tkachenko mode and the optical Tkachenko mode, which have k^2 and k dispersion, respectively. Both the two gapped modes and the optical Tkachenko mode have isotropic behavior, however, the underlying square lattice causes the acoustic Tkachenko mode dispersion to be anisotropic. The anisotropy of the acoustic Tkachenko mode is more transparent when written as

$$\omega_T^{\rm ac} = \sqrt{2(1+\alpha)\left[C_u \cos^2(2\theta) + C_v \sin^2(2\theta)\right]}\frac{k'^2}{2\Omega}. \tag{4.78}$$

The acoustic mode spectrum is plotted in Fig. 4.7 for two different values of α. We notice that depending on the elastic constants two different types of softening happens for the acoustic Tkachenko modes. If $C_u = 0$, then the acoustic modes along the directions

$$\theta = 0, \pi/2, \pi, 3\pi/2 \tag{4.79}$$

become soft. We see from the numerical fit that C_u becomes zero near $\alpha = 0.3733$ and these soft modes control the dynamics of the second-order phase transition to the rhombic lattice. The other possibility for soft mode formation is when $C_v = 0$. In this case the soft acoustic modes are along the directions

$$\theta = \pi/4, 3\pi/4, 5\pi/4, 7\pi/4. \tag{4.80}$$

These soft modes, then, signal the second-order phase transition to the rectangular lattice, at $\alpha = 0.9256$.

4.7 Rectangular lattice

When the interactions between the components are close to the interactions within each component, the energetically favorable lattice becomes a rectangular lattice. The rectangular lattice has $a_* = b_* = 1/2$, so vortices of one-component are placed at the centers of the rectangles formed by the vortices of the other component. The ratio of the long side of the rectangles to their short side, v_*, increases with increasing α (see Fig. 4.2).

The elastic energy can once again be separated as

$$E_{\text{elastic}} = E^{\text{ac}}_{\text{elastic}} + E^{\text{op}}_{\text{elastic}}. \tag{4.81}$$

Here, we express the acoustic part of the elastic energy as

$$E^{\text{ac}}_{\text{elastic}} = \frac{1}{2}\int d^2r \left[C_1^{\text{ac}} \left(\frac{\partial \epsilon_+^x}{\partial x} - \frac{\partial \epsilon_+^y}{\partial y} \right)^2 + C_2^{\text{ac}} \left(\frac{\partial \epsilon_+^x}{\partial y} + \frac{\partial \epsilon_+^y}{\partial x} \right)^2 \right], \tag{4.82}$$

a form that is essentially the same as the square lattice, as the hydrostatic compression modulus is zero. The optical part is

$$E^{\text{op}}_{\text{elastic}} = \int d^2r \left[C_1^{\text{op}} \left(\epsilon_-^x \right)^2 + C_2^{\text{op}} \left(\epsilon_-^y \right)^2 \right]. \tag{4.83}$$

For the acoustic modes, we define the dimensionless elastic constants

$$\tilde{C}_1^{\text{ac}} = \frac{C_1^{\text{ac}}}{gn^2}, \qquad \tilde{C}_2^{\text{ac}} = \frac{C_2^{\text{ac}}}{gn^2}, \tag{4.84}$$

and fit the acoustic part of the elastic energy to the form

$$E^{\text{ac}}_{\text{elastic}} = \frac{gn^2}{2} \left[C_u (u - u_*)^2 + C_v (v - v_*)^2 \right], \tag{4.85}$$

which results in

$$\tilde{C}_1^{\text{ac}} = v_*^2 C_v, \qquad \tilde{C}_2^{\text{ac}} = v_*^2 C_u. \tag{4.86}$$

The numerical results for elastic constants C_u and C_v are given in Fig. 4.8.

As a result, we calculate the acoustic Tkachenko mode frequency

$$\omega_T^{\text{ac}} = \sqrt{\frac{1+\alpha}{2}} \sqrt{\tilde{C}_1^{\text{ac}} \sin^2(2\theta) + \tilde{C}_2^{\text{ac}} \cos^2(2\theta)} \frac{k'^2}{\Omega}, \tag{4.87}$$

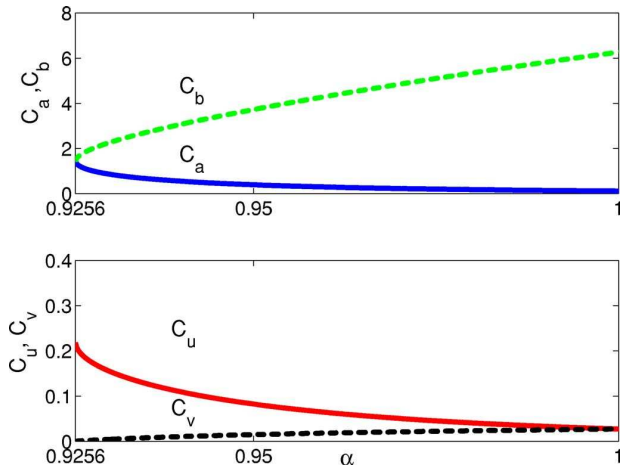

Figure 4.8: Elastic constants (C_a, C_b, C_u, C_v) of rectangular lattice. The upper figure shows optical elastic constants(C_a, C_b). As $\alpha \to 1$, C_a vanishes. The lower figure shows acoustic elastic constants (C_u, C_v). As $\alpha \to 1$, $C_u \to C_v$ and there remains only one acoustic elastic constant similar to the one-component triangular lattice.

and the acoustic inertial mode frequency

$$(\omega_I^{\rm ac})^2 = 4\Omega^2 + [1 + \alpha + 2(\tilde{C}_1^{\rm ac} + \tilde{C}_2^{\rm ac})]k'^2. \tag{4.88}$$

For the optical modes, we nondimensionalize

$$\tilde{C}_1^{\rm op} = \frac{d_1^2}{gn^2} C_1^{\rm op}, \qquad \tilde{C}_2^{\rm op} = \frac{d_2^2}{gn^2} C_2^{\rm op}, \tag{4.89}$$

where d_1 and d_2 are the sides of the rectangular unit cell with

$$d_1^2 = \frac{\pi}{\Omega m v_*}, \qquad d_2^2 = \frac{\pi v_*}{\Omega m}. \tag{4.90}$$

When the elastic energy is fitted to the numerical form

$$E_{\rm elastic}^{\rm op} = \frac{gn^2}{2}\left[C_a(a-a_*)^2 + C_b(b-b_*)^2\right], \tag{4.91}$$

we obtain

$$\tilde{C}_1^{\rm op} = \frac{C_a}{2}, \qquad \tilde{C}_2^{\rm op} = \frac{C_b}{2}, \tag{4.92}$$

The dependence of C_a and C_b on α is plotted in Fig. 4.8.

As a result of the calculation, we obtain the optical Tkachenko mode dispersion

$$\omega_T^{\rm op} = \sqrt{\frac{1-\alpha}{\pi}\frac{gn}{\Omega}}\sqrt{\frac{\tilde{C}_2^{\rm op}}{v_*}\cos^2(\theta) + \tilde{C}_1^{\rm op} v_* \sin^2(\theta)}\, k', \tag{4.93}$$

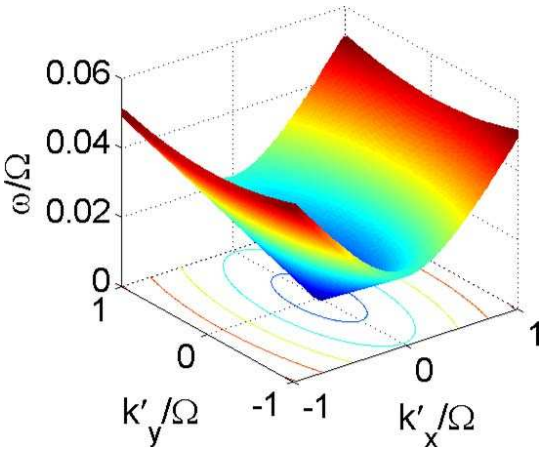

Figure 4.9: Dispersion relation of the optical Tkachenko mode of the rectangular lattice, Eq. (4.93), for $\alpha = 0.95$, $\frac{gn}{\Omega} = 0.1$. The underlying contour plot reflects the symmetry of the rectangular lattice.

and the inertial mode frequencies

$$(\omega_I^{\rm op})^2 = 4\Omega^2 \left[1 + \frac{gn}{\pi\Omega}\left(v_* \tilde{C}_1^{\rm op} + \frac{1}{v_*}\tilde{C}_2^{\rm op}\right)\right] + (1-\alpha)k'^2. \tag{4.94}$$

A number of important conclusions can be deduced from the above results. First of all, both the acoustic and optical Tkachenko modes are anisotropic, while the inertial modes are isotropic for the rectangular lattice. While the anisotropy of the acoustic Tkachenko mode, is similar to the anisotropy obtained for the square lattice, the anisotropy of the optical modes can be understood by a different mechanism. The rectangular lattice can be thought of as alternating planes of vortices of different components. It is easier to move the vortices in these planes, rather than perpendicular to these planes. A typical dispersion of optical Tkachenko modes is given in Fig. 4.9.

As a second property, we see that near $\alpha = 0.9256$ there is a soft acoustic mode, signaling a second-order transition to the square lattice. Thus both sides of the transition from square to rectangular lattice have a soft acoustic mode.

When intercomponent interaction is equal in strength to the interaction within the components, i.e., $\alpha = 1$, a number of interesting phenomena are expected. First, at $\alpha = 1$, there is no distinction between different components, and one would expect the results to be the same as that of a single-component vortex

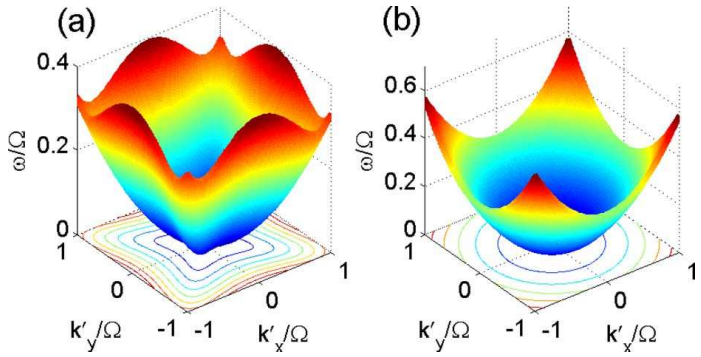

Figure 4.10: Dispersion relation of the acoustic Tkachenko modes of the rectangular lattice, Eq. (4.87) for $\alpha = 0.95$ (a) and for $\alpha = 1.0$ (b). At $\alpha = 1.0$, the dispersion relation becomes isotropic. The similarity between (a) and Fig. 4.7(b) is due to the second-order phase transition between square and rectangular lattices.

lattice. Indeed, at this point, $v_* = \sqrt{3}$, and the resulting rectangular lattice is equivalent to a single-component triangular lattice. Furthermore, the acoustic mode spectrum becomes isotropic exactly at this point, as can be seen in Fig. 4.10.

However, the point $\alpha = 1$, where the intercomponent interaction is the same as the interaction between the components, is special in another way. For a nonrotating two-component BEC, there is an instability towards phase-separation at this point. In previous studies of two-component BECs with vortex lattices, this instability was not observed. However, we find that at $\alpha = 1$ the optical Tkachenko mode becomes soft, and the system is unstable beyond $\alpha = 1$. This is reflected in the $\sqrt{1-\alpha}$ term, in the dispersion relation Eq. (4.93). Thus we find that there is an instability beyond $\alpha = 1$, for rapidly rotating two-component condensates. As previous studies of this system did not take the coupling between the vortex movement and density oscillations into account, it is not surprising that this instability was not observed.

Although we find that there is an instability at $\alpha = 1$, it is not clear that this instability leads directly to phase-separation. The analog of the sound mode that is unstable in a nonrotating system is the optical inertial mode. As this mode has a gap, there is no instability in the long-wavelength. We find that the

dispersion of the optical inertial mode has a k^2 term with a negative coefficient, but this is not sufficient to claim that there will be an instability at a finite value of k, as higher-order terms such as k^4 may prevent the dispersion from reaching zero frequency. Instead there may be a phase with partial phase-separation and disordered distribution of vortices beyond $\alpha = 1$. Further investigation of this instability is needed to determine the nature of the phase beyond $\alpha = 1$.

4.8 Rhombic lattice

The final lattice type we consider is the rhombic lattice, which is the minimum-energy configuration for $0.1724 < \alpha < 0.3733$. This lattice is an intervening phase between the interlaced triangular lattice and the square lattice discussed in previous sections. At $\alpha = 0.1724$ there is a first-order transition from the interlaced triangular lattice, where a_* and b_* change discontinuously from $1/2$ to

$$a_* = b_* = \frac{1}{3}. \tag{4.95}$$

The unit cell also becomes a rhombus, while the acute angle of the rhombus η continuously changes from 67.96° to 90°. A plot of the lattice geometry and the change of η is given in Fig. 4.2.

The rhombic lattice has twofold (reflection) symmetry along the axis that makes an angle $\eta/2$ with the primitive basis vectors. However, instead of expressly taking advantage of this symmetry, we use a general form for the elastic energy. Writing

$$E_{\text{elastic}} = E^{\text{ac}}_{\text{elastic}} + E^{\text{op}}_{\text{elastic}}, \tag{4.96}$$

we use

$$\begin{aligned} E^{\text{ac}}_{\text{elastic}} = \frac{1}{2}\int d^2r [C_1^{\text{ac}}(\frac{\partial \epsilon_+^x}{\partial x} - \frac{\partial \epsilon_+^y}{\partial y})^2 + C_2^{\text{ac}}(\frac{\partial \epsilon_+^x}{\partial y} + \frac{\partial \epsilon_+^y}{\partial x})^2 \\ + C_3^{\text{ac}}(\frac{\partial \epsilon_+^x}{\partial y} + \frac{\partial \epsilon_+^y}{\partial x})(\frac{\partial \epsilon_+^x}{\partial x} - \frac{\partial \epsilon_+^y}{\partial y})], \end{aligned}$$

and

$$E^{\text{op}}_{\text{elastic}} = \int d^2r \left[C_1^{\text{op}} \left(\epsilon_-^x\right)^2 + C_2^{\text{op}} \left(\epsilon_-^y\right)^2 + C_3^{\text{op}} \epsilon_-^x \epsilon_-^y \right]. \tag{4.97}$$

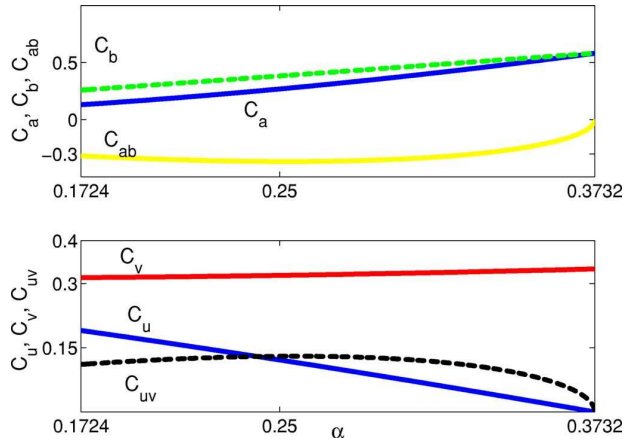

Figure 4.11: Optical elastic constants [upper, Eq. (4.106)] and acoustic elastic constants [lower, Eq. (4.99)] of rhombic lattice with respect to α. As $\alpha \to 0.3732$, $C_a \to C_b$, and C_u, C_v vanish, leaving two optical elastic constants, and one acoustic elastic constant for the square lattice. In the opposite limit $\alpha \to 0.1724$, six elastic constants remain due to the discontinuity in the transition to interlaced triangular lattice.

For the acoustic modes, we define dimensionless quantities

$$\tilde{C}_1^{\rm ac} = \frac{C_1^{\rm ac}}{gn^2}, \qquad \tilde{C}_2^{\rm ac} = \frac{C_2^{\rm ac}}{gn^2}, \qquad \tilde{C}_3^{\rm ac} = \frac{C_3^{\rm ac}}{gn^2}, \tag{4.98}$$

and fit the acoustic part of the elastic energy to the form

$$E_{\rm elastic}^{\rm ac} = \frac{gn^2}{2}\left[C_u(u-u_*)^2 + C_v(v-v_*)^2 + C_{uv}(u-u_*)(v-v_*)\right], \tag{4.99}$$

which yields

$$\tilde{C}_1^{\rm ac} = v_*^2 C_v, \qquad \tilde{C}_2^{\rm ac} = v_*^2 C_u, \qquad \tilde{C}_3^{\rm ac} = -v_*^2 C_{uv}. \tag{4.100}$$

The numerical results for elastic constants C_u, C_v, and C_{uv} are given in Fig. 4.11.

We find the acoustic inertial mode dispersion

$$(\omega_I^{\rm ac})^2 = 4\Omega^2 + [1+\alpha+2(\tilde{C}_1^{\rm ac}+\tilde{C}_2^{\rm ac})]k'^2, \tag{4.101}$$

and the acoustic Tkachenko mode dispersion

$$\omega_T^{\rm ac} = \sqrt{\frac{1+\alpha}{2}}\sqrt{4\tilde{C}_1^{\rm ac}\frac{k_x^2k_y^2}{k^4} + \tilde{C}_2^{\rm ac}\frac{(k_x^2-k_y^2)^2}{k^4} + 2\tilde{C}_3^{\rm ac}\frac{k_xk_y(k_y^2-k_x^2)}{k^4}}\,\frac{k'^2}{\Omega}. \tag{4.102}$$

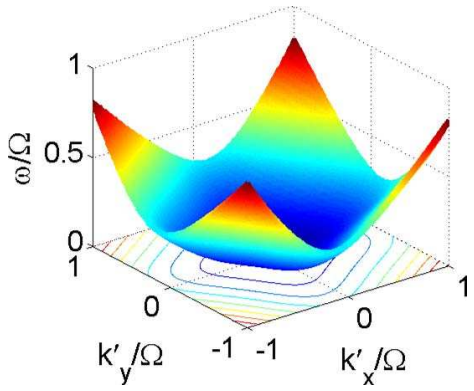

Figure 4.12: Dispersion relation of the acoustic Tkachenko mode of the rhombic lattice, Eq. (4.102), for $\alpha = 0.2$. The anisotropy reflects the twofold symmetry of the rhombic lattice (see Fig. 4.13).

The anisotropy of the Tkachenko mode is more transparent when represented in terms of θ, the angle from the $\hat{x}$ axis,

$$\omega_T^{\rm ac} = \sqrt{\frac{1+\alpha}{2}}\sqrt{\tilde{C}_1^{\rm ac}\sin^2(2\theta) + \tilde{C}_2^{\rm ac}\cos^2(2\theta) - \tilde{C}_3^{\rm ac}\sin(4\theta)}\frac{k'^2}{\Omega}. \tag{4.103}$$

For the optical modes, we define the dimensionless elastic constants,

$$\tilde{C}_1^{\rm op} = \frac{d^2}{gn^2}C_1^{\rm op}, \qquad \tilde{C}_2^{\rm op} = \frac{d^2}{gn^2}C_2^{\rm op}, \qquad \tilde{C}_3^{\rm op} = \frac{d^2}{gn^2}C_3^{\rm op}, \tag{4.104}$$

where the side length of the rhombus d is

$$d^2 = \frac{\pi}{\Omega m \sin(\eta)}. \tag{4.105}$$

We use a numerical fit to the energy of the general form

$$\begin{aligned} E_{\rm elastic}^{\rm op} = \frac{gn^2}{2}\{&C_{ax}[(a-a_*)+u_*(b-b_*)]^2 + C_{by}v_*^2(b-b_*)^2 \\ &+C_{ab}[(a-a_*)+u_*(b-b_*)]v_*(b-b_*)\}, \end{aligned}$$

which yields

$$\tilde{C}_1^{\rm op} = \frac{C_{ax}}{2}, \qquad \tilde{C}_2^{\rm op} = \frac{C_{by}}{2}, \qquad \tilde{C}_3^{\rm op} = \frac{C_{ab}}{2}, \tag{4.106}$$

The dependence of C_{ax}, C_{by}, and C_{ab} on α is plotted in Fig. 4.11.

We find the optical inertial mode

$$(\omega_I^{\rm op})^2 = 4\Omega^2\left[1 + \frac{gn}{\pi\Omega}\sin(\eta)\left(\tilde{C}_1^{\rm op} + \tilde{C}_2^{\rm op}\right)\right] + (1-\alpha)k'^2, \tag{4.107}$$

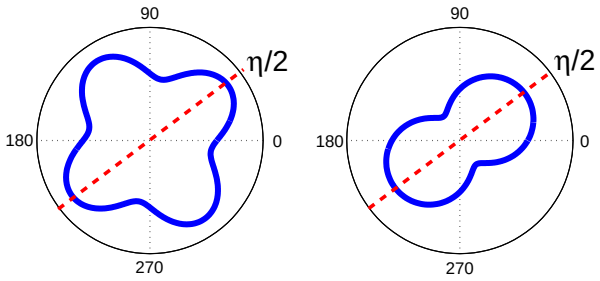

Figure 4.13: (Color) Polar plot of the frequency of the acoustic [left, Eq. (4.102)] and the optical [right, Eq. (4.108)] Tkachenko modes for the rhombic lattice ($k = 0.1$, $\frac{gn}{\Omega} = 0.1$, $\alpha = 0.2$). $\eta/2$ is the opening angle of the rhombic unit cell at $\alpha = 0.2$.

and the optical Tkachenko mode

$$\omega_T^{\mathrm{op}} = \sqrt{\frac{1-\alpha}{\pi}\frac{gn}{\Omega}\sin(\eta)}\sqrt{\tilde{C}_2^{\mathrm{op}}\cos^2(\theta) + \tilde{C}_1^{\mathrm{op}}\sin^2(\theta) - \frac{1}{2}\tilde{C}_3^{\mathrm{op}}\sin(2\theta)}\,k'. \quad (4.108)$$

For the rhombic lattice, both the acoustic and the optical Tkachenko modes are anisotropic. A typical dispersion for the acoustic Tkachenko modes is displayed in Fig. 4.12. In the calculation above we have not implicity assumed the twofold symmetry of the rhombic lattice, however, the resulting dispersion relations respect this symmetry. As an example the polar plot of optical and acoustic mode frequencies is given in Fig. 4.13. This symmetry can be viewed as a validation of the numerical approach we use to calculate the elastic coefficients.

Another property of the Tkachenko modes of the rhombic lattice is that the transition to the square lattice at $\alpha = 0.3733$ is accompanied by a soft acoustic mode. However, the first-order transition to the triangular lattice does not have any soft acoustic or optical Tkachenko mode.

4.9 Structural phase transitions

The two-component vortex lattice system has five different equilibrium lattice types and four structural phase transitions between them. In this section, we comment on the interplay between these transitions and the Tkachenko modes of

the lattice. Our aim is to give an overall picture of the physics in this system as the intercomponent interaction α is varied. We start from $\alpha = -1$, and consider all transitions as α is increased.

For $\alpha < -1$, the two-component BEC system is unstable towards collapse due to the strength of attraction between the components. This instability is apparent in the Tkachenko mode spectrum of the overlapped triangular lattice for α values greater than but close to -1. Here there is a soft acoustic Tkachenko mode, as discussed in Sec. 4.4.

At $\alpha = 0$, when there is no interaction between the two-components of the BEC, the vortex lattice geometry changes from overlapped triangular lattice to the interlaced triangular lattice. This first-order transition leaves the unit cell geometry the same, however, there is a discontinuous jump in the relative positions of vortices within the unit cell. On both sides of the transition there is a soft optical Tkachenko mode. Thus the reordering inside the unit cell is accompanied by a soft long-wavelength mode as expected.

As the intercomponent repulsion is increased further, there is a first-order phase transition from the interlaced triangular lattice to the rhombic lattice, at $\alpha = 0.1724$. In this transition, both the unit cell geometry and the positions of vortices inside the unit cell change discontinuously. We find no signature of this transition in the long-wavelength optical or acoustic modes. The instability mechanism causing this transition must include both optical and acoustic Tkachenko modes, and must take place at wavelengths comparable to the lattice spacing. Thus this instability is not captured by our linear, long-wavelength approach.

Between $\alpha = 0.1724$ and $\alpha = 0.3733$ the rhombic lattice is the minimum-energy configuration, and at $\alpha = 0.3733$ there is a second-order phase transition to the square lattice. On both sides of this transition there is a soft acoustic Tkachenko mode. The acoustic modes have anisotropic dispersion for both square and rhombic lattices, and the soft mode has a wave vector $\vec{k}$, that is parallel to the primitive lattice basis vectors $\vec{a}_1 = d\hat{x}$, or $\vec{a}_2 = d\hat{y}$. As in the structural phase transitions of solids, a second-order phase transition is accompanied by a soft acoustic mode.

The final structural phase transition between different lattice geometries takes place at $\alpha = 0.9256$, between the square and rectangular lattices. This is a second-order phase transition, and we find that there is a soft acoustic Tkachenko mode on both sides of the transition. The soft mode has a wave vector $\vec{k}$ that makes an angle of $\pi/4$ with the primitive lattice basis vectors, $\vec{k} \parallel (\vec{a}_1 + \vec{a}_2)$.

For a nonrotating system there is a phase-separation instability at $\alpha = 1$. We find that at this point the optical Tkachenko modes of the rotating system become soft. However, as discussed in Sec. 4.7, it is not clear if this instability directly leads to phase-separation, or to another phase.

Chapter 5

Conclusions and Future Work

This is the concluding chapter of the thesis where all the result are summarized. In the first section our results for the stationary condensates are explained briefly. In the following section, we explain our results for the rotating condensates which are mainly given in Chapter 4. The last section is devoted to possible extensions to this thesis work.

5.1 Similariton Function

In Section 2.2.3, we have given our results that are obtained using the similariton function. Briefly, we have solved GPE with any kind of symmetry using a variational ansatz and compared our results with the numerical solutions. However, we have only solved time independent GPE, but the extension to time-dependent one is not so hard. Similariton function can also be used to solve modified GPE which is used for high densities [31, 9, 29]. There will be no need to change the form of the similariton function, but only change is in the GPE and it will make calculations a little bit longer. It is also possible to obtain solutions for vortex states. A variational function with cylindrical symmetry should have

the form,

$$\psi(\rho, z) = C\rho^l \exp(-\sum_{k=1}^{n_\rho} \frac{(\rho/d_\rho)^{2k}}{2k}) \exp(-\sum_{k=1}^{n_z} \frac{(z/d_z)^{2k}}{2k}), \tag{5.1}$$

where l is an additional variational parameter that takes integer values.

5.2 Tkachenko Modes for Spinor BECs

We considered a rapidly rotating two-component BEC, and calculated the Tkachenko mode dispersion relations for different lattice geometries. We find that a two-component vortex lattice has two branches of Tkachenko modes, which we call acoustic and optical Tkachenko modes in analogy with phonons. The acoustic Tkachenko modes have k^2 dispersion at long-wavelengths while the optical Tkachenko modes have linear, k, dispersion. For all lattice types other than triangular lattices, the dispersion relations are anisotropic. By investigating the behavior of Tkachenko modes near structural phase transitions, we identified the soft modes that are responsible for the phase transitions. Out of the four structural phase transitions two are of second-order, while the remaining two are first-order. The second-order transitions are accompanied by the softening of an acoustic mode. For one of the first-order phase transitions we identified a soft optical Tkachenko mode, while for the other first-order transition, no such long-wavelength mode was found. We also found that if the intercomponent repulsion is stronger than the interactions within each component, the vortex lattice is unstable. This instability may lead to phase-separation, as is the case for a nonrotating two-component BEC.

In a recent experiment at JILA [74], a rapidly rotating two-component Rb condensate was created. It was found that the equilibrium vortex lattice configuration is square. Furthermore, when the lattice was perturbed, a Tkachenko like mode was observed, however, this mode was found to be heavily damped, thus it has not been possible to measure the Tkachenko mode frequencies.

There are three important points to consider when comparing our results with this experiment. First the interaction parameters for the Rb system used

in the experiment are different from what was considered in this paper, most importantly, interaction parameters within each component are not the same,

$$g_{11} \neq g_{22}. \tag{5.2}$$

In this case, one would expect the acoustic and optical Tkachenko modes to be coupled. However, this coupling should be relatively small, as

$$\frac{2(g_{11} - g_{22})}{g_{11} + g_{22}} \approx 0.05. \tag{5.3}$$

When the interaction strengths within each component is different, we may redefine

$$\alpha = \frac{g_{12}}{\sqrt{g_{11} g_{22}}}, \tag{5.4}$$

which for the Rb system is very close to 1. Although the calculations in the LLL indicate that a rectangular lattice is more favorable, experimentally the lattice structure is found to be a square within experimental error. This implies, as a second point, that one must take into account that the experimental system is not fully in the LLL regime. As the third and final point, the experimental system is of finite extent. The overall density profile in the system is affected by the finite size of the system and may cause in shifts in vortex positions [15]. More importantly, the coupling between vortex oscillations and the density modes, coupled with other loss mechanisms, damp the Tkachenko modes.

The above limitations prevent a direct quantitative comparison of data with the theory presented in this paper. There are, however, some important qualitative conclusions that can be drawn. A puzzling result of the experiment is that the Tkachenko excitations in the two-component BEC are more heavily damped compared to a single-component system. It is thought that the main damping mechanism is the coupling to surface modes near the edges of the cloud, but this mechanism would be independent of whether one is using a one-component or a two-component condensate. We believe that there are two effects that contribute to this apparently high damping rate. The method used in the experiment to excite Tkachenko modes is to focus a resonant laser beam onto the center of the condensate. This method excites Tkachenko modes isotropically, giving equal weight to every direction. However, our calculations show that Tkachenko modes

in a square (or rectangular) lattice are anisotropic. This anisotropy is very pronounced if the system is close to square to rectangular structural phase transition, which the experimental system could be as indicated by the ratio of its interaction strengths. When Tkachenko modes are excited isotropically, because oscillations along different directions have different frequencies, there will be a significant dephasing effect. We believe a significant part of the observed damping is due to this dephasing. A second effect is that, because of the coupling between the acoustic and the optical modes, during the excitation optical Tkachenko modes are also excited. By making measurements on the vortex positions of one-component it is not possible to distinguish one type of oscillation from the other. We believe, if the excitation mechanism can be made anisotropic, for example by using a resonant laser with an elliptical focus, it should be possible to observe smaller damping rates.

It is also interesting to note that it should be possible to measure optical Tkachenko modes, using the same interference technique used in the experiment to prove that the vortices form interlaced lattices. An optical Tkachenko mode, once excited, would cause oscillations in the visibility of the "vortex lattice interference" fringes.

Another interesting point is that, we have identified an isotropic Tkachenko mode for the square lattice at $\alpha = \frac{\sqrt{(2)}}{2}$ [47]. At this value of α, the ratio of the distance between the vortices of different components to the distance between the vortices of the same component is the same. The isotropy of acoustic Tkachenko mode only at this point may be a result of a simple $\frac{1}{r}$ repulsive potential between vortices.

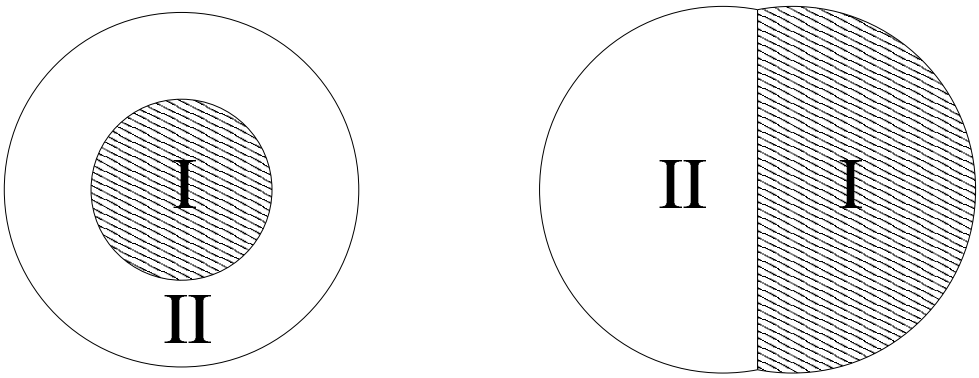

Figure 5.1: Symmetric(left) and asymmetric(right) phase configurations for two-component BEC.

5.3 Future Work

5.3.1 Phase Separation for $\alpha \geq 1$

Phase separation for nonrotating binary condensates are well studied both experimentally and theoretically, and it is known from these studies that phase separation occurs for $\alpha = \frac{g_{12}}{\sqrt{g_{11}g_{22}}} > 1$. The signal of this separation is imaginary density oscillation frequencies, and the stable configuration is the symmetric case shown in Fig. 5.1, where the inner component is the one with less repulsion.

We found a similar instability for $\alpha > 1$ since acoustic Tkachenko mode becomes imaginary. Therefore, we expect a similar phase separation for this repulsive regime. However we could not find the least energetic configuration. As suggested by Ueda *et al.* [44], we found that at $\alpha = 1$ many different configurations have the same energy. We calculated the energy for the symmetric configuration shown in Fig. 5.1 where the inner component carries doubly quantized vortices in a triangular array. The energy we found is very close to the interlaced rectangular lattice configuration explained in Section 4.7.

5.3.2 Optical Lattices

One of the most important development in the cold atom physics after demonstration of BEC is placing atoms in optical lattices. Experimentalist can now load BECs in optical lattices [59] and phase transitions such as Mott insulator-superfluid transition can be observed [33]. Therefore, many theoretical papers are appearing about BECs in optical lattices. For our interest in this thesis we look at rotating condensates which are put in an optical potential either in the z direction or in the xy plane. For the former case the change of the vortex lattice structure due to optical lattice potential can be found with the LLL approach presented in this thesis. For the latter case, there is a work of Zai *et al.* [77] investigating the phase diagram of double layer condensates with large number of vortices using a similar approach to ours. A future work can be calculating Tkachenko modes using the methods presented in this thesis.

Bibliography

[1] http://cua.mit.edu/ketterle_group/Nice_pics.htm.

[2] https://ucan.physics.utoronto.ca/News.

[3] J. R. Abo-Shaeer, C. Raman, and W. Ketterle. Formation and decay of vortex lattices in Bose-Einstein condensates at finite temperatures. *Phys. Rev. Lett.*, 88(7):070409, 2002.

[4] J. R. Abo-Shaeer, C. Raman, J. M. Vogels, and W. Ketterle. Observation of vortex lattices in Bose-Einstein condensates. *Science*, 292(5516):476, 2001.

[5] A. A. Abrikosov. On the magnetic properties of superconductors of the second group. *Sov. Phys. JETP*, 5(1174), 1957.

[6] M. H. Anderson, J. R. Ensher, M. R. Matthews, C. E. Wieman, and E. A. Cornell. Evidence for Bose-Einstein condensation in a dilute atomic vapor. In Massimo Inguscio, Maria Allegrini, and Antonio Sasso, editors, *Laser Spectroscopy, XII International Conference*, page 3. World Scientific, 1995.

[7] M. R. Andrews, M.-O. Mewes, N. J. van Druten, D. S. Durfee, D. M. Kurn, and W. Ketterle. Direct, nondestructive observation of a Bose condensate. *Science*, 273(0):84, 1996.

[8] L. O. Baksmaty, S. J. Woo, S. Choi, and N. P. Bigelow. Tkachenko waves in rapidly rotating Bose-Einstein condensates. *Phys. Rev. Lett.*, 92(16):160405, 2004.

[9] A. Banerjee and M. P. Singh. Ground-state properties of a trapped Bose gas beyond the mean-field approximation. *Phys. Rev. A*, 64:063604, 2001.

[10] W. Bao and W. Tang. Ground-state solution of Bose-Einstein condensate by directly minimizing the energy functional. *Journal of Computational Physics*, 187(1):230–254, 2003.

[11] G. I. Barenblatt. *Scaling, Self-similarity, and Intermediate Asymptotics*. Cambridge University Press, Cambridge, 1996.

[12] G. Baym. Tkachenko modes of vortex lattices in rapidly rotating Bose-Einstein condensates. *Phys. Rev. Lett.*, 91(11):110402, 2003.

[13] G. Baym and E. Chandler. The hydrodynamics of rotating superfluids. *J. Low Temp. Phys.*, 50(57), 1983.

[14] G. Baym and C. J. Pethick. Ground-state properties of magnetically trapped Bose-condensed rubidium gas. *Phys. Rev. Lett.*, 76(1):6, 1996.

[15] G. Baym and C. J. Pethick. Vortex core structure and global properties of rapidly rotating Bose-Einstein condensates. *Phys. Rev. A*, 69(4):043619, 2004.

[16] J. L. Bohn, B.D. Esry, and C.H. Greene. Effective potentials for dilute Bose-Einstein condensates. *Phys. Rev. A*, 58(1):584–597, 1998.

[17] S. Bose. Plancks Gesetz und Lichtquantenhypothese. *Z. Phys.*, 26(3):178, 1924.

[18] C. C. Bradley, C. A. Sackett, and R. G. Hulet. Bose-Einstein condensation of lithium: Observation of limited condensate number. *Phys. Rev. Lett.*, 78(6):985, 1997.

[19] I. Coddington, P. Engels, V. Schweikhard, and E. A. Cornell. Observation of Tkachenko oscillations in rapidly rotating Bose-Einstein condensates. *Phys. Rev. Lett.*, 91(10):100402, 2003.

[20] I. R. Coddington. *Vortices in a Highly Rotating Bose Condensed Gas*. PhD thesis, JILA, 2004.

[21] N. R. Cooper, N. K. Wilkin., and J. M F. Gunn. Quantum phases of vortices in rotating Bose-Einstein condensates. *Phys. Rev. Lett.*, 87(12):120405, 2001.

[22] Eric Cornell. Very cold indeed: The nanokelvin physics of Bose-Einstein condensation. *J. Res. Natl. Inst. Stand. Tech.*, 101(4):419, 1996.

[23] M. Cozzini, L. P. Pitaevskii, and S. Stringari. Tkachenko oscillations and the compressibility of a rotating Bose-Einstein condensate. *Phys. Rev. Lett.*, 92(22):220401, 2004.

[24] M. Cozzini, S. Stringari, and C. Tozzo. Vortex lattices in Bose-Einstein condensates: From the thomas-fermi regime to the lowest-Landau-level regime. *Phys. Rev. A*, 73(2):023615, 2006.

[25] M. Crescimanno, C. G. Kaoy, and R. Peterson. Limits to sympathetic evaporative cooling of a two-component Fermi gas. *Phys. Rev. A*, 61:053602, 2000.

[26] F. Dalfovo and S. Stringari. Bosons in anisotropic traps: Ground state and vortices. *Phys. Rev. A*, 53(4):2477, 1996.

[27] M. Edwards and K. Burnett. Numerical solution of the nonlinear Schrödinger equation for small samples of trapped neutral atoms. *Phys. Rev. A*, 51(2):1382, 1995.

[28] A. Einstein. Quantentheorie des einatomigen idealen Gases. Zweite Abhandlung. *Sitzungber. Preuss. Akad. Wiss.*, 1925:3, 1925.

[29] E. Erdemir and B. Tanatar. q-gaussian trial function in high density Bose-Einstein condensates. *Physica A: Statistical Mechanics and its Applications*, 322:449–455, 2003.

[30] U. Essmann and H. Trauble. The direct observation of individual flux lines in type ii superconductors. *Physics Letters A*, 24(10):526–527, 1967.

[31] A. Fabrocini and A. Polls. Beyond the Gross-Pitaevskii approximation: Local density versus correlated basis approach for trapped bosons. *Phys. Rev. A*, 60(3):2319, 1999.

[32] A. L. Fetter. Variational study of dilute Bose condensate in a harmonic trap. *J. Low Temp. Phys.*, 106(5/6):643, 1997.

[33] M. Greiner, O. Mandel, T. Esslinger, T. W. Hänsch, and Immanuel Bloch. Quantum phase transition from a superfluid to a Mott insulator in a gas of ultracold atoms. *Nature*, 415:39, 2002.

[34] E. P. Gross. *Nuovo Cimento*, 20(454), 1961.

[35] E. P. Gross. *J. Math. Phys.*, 4(195), 1963.

[36] P. C. Haljan. *Vortices in a Bose-Einstein Condensate*. PhD thesis, JILA, 2003.

[37] P. C. Haljan, B. P. Anderson, I. Coddington, and E. A. Cornell. Use of surface-wave spectroscopy to characterize tilt modes of a vortex in a Bose-Einstein condensate. *Phys. Rev. Lett.*, 86(14):2922, 2001.

[38] P. C. Haljan, I. Coddington, P. Engels, and E. A. Cornell. Driving Bose-Einstein-condensate vorticity with a rotating normal cloud. *Phys. Rev. Lett.*, 87(21):210403, 2001.

[39] G. Heckenblaikner, E. Hodby, S. A. Hopkins, O. M. Maragó, and C. J. Foot. Direct observation of irrotational flow and evidence of superfluidity in a rotating Bose-Einstein condensate. *Phys. Rev. Lett.*, 88(7):070406, 2002.

[40] Tin-Lun Ho. Bose-Einstein condensates with large number of vortices. *Phys. Rev. Lett.*, 87(6):060403, 2001.

[41] F. O. Ilday, J. R. Buckley, W. G. Clark, and F. W. Wise. Self-similar evolution of parabolic pulses in a laser. *Phys. Rev. Lett.*, 92(21):213902, 2004.

[42] K. N. Ilinski and A. Moroz. Aspect ratio analysis for ground states of bosons in anisotropic traps. *Czech. J. Phys.*, 46(S1):549, 1996.

[43] C. Jirauschek and F. O. Ilday. Theory of the self-similar laser oscillator. (to be published), 2006.

[44] K. Kasamatsu, M. Tsubota, and M. Ueda. Vortex phase diagram in rotating two-component Bose-Einstein condensates. *Phys. Rev. Lett.*, 91(15):150406, 2003.

[45] M. Keçeli, F. O. Ilday, and M. O. Oktel. Similariton ansatz for Gross-Pitaevskii equation. (to be published), 2006.

[46] M. Keçeli and M. O. Oktel. Tkachenko modes and structural phase transitions of the vortex lattice of a two-component Bose-Einstein condensate. *Phys. Rev. A*, 73(2):023611, 2006.

[47] M. Keçeli and M. O. Oktel. Tkachenko modes of the square vortex lattice in a two-component Bose-Einstein condensate. (in press), 2006.

[48] W. Ketterle. Experimental studies of Bose-Einstein condensation. *Phys. Today*, 52(12):30, 1999.

[49] C. Kittel. *Introduction to Solid State Physics*. Number 402. Jonh Wiley & Sons, New York, 7. edition, 1996.

[50] M. Kozuma, L. Deng, E. W. Hagley, J. Wen, R. Lutwak, K. Helmerson, S. L. Rolston, and W. D. Phillips. Coherent splitting of Bose-Einstein condensed atoms with optically induced Bragg diffraction. *Phys. Rev. Lett.*, 82(5):871, 1999.

[51] L. D. Landau and E. M. Lifshitz. *Theory of Elasticity*. Number 35-37. Oxford, Pergamon, 1970.

[52] E. Lundh, C. J. Pethick, and H. Smith. Zero-temperature properties of a trapped Bose-condensed gas: Beyond the Thomas-Fermi approximation. *Phys. Rev. A*, 55(3):2126, 1997.

[53] K. W. Madison, F. Chevy, W. Wohlleben, and J. Dalibard. Vortex formation in a stirred Bose-Einstein condensate. *Phys. Rev. Lett.*, 84(5):806, 2000.

[54] R. Malvin. Long period oscillations in rotating neutron stars. *Nature*, 225(5233):619–620, 1970.

[55] M. R. Matthews, B. P. Anderson, P. C. Haljan, D. S. Hall, C. E. Wieman, and E. A. Cornell. Vortices in a Bose-Einstein condensate. *Phys. Rev. Lett.*, 83(13):2498, 1999.

[56] T. Mizushima, Y. Kawaguchi, K. Machida, T. Ohmi, T. Isoshima, and M. M. Salomaa. Collective oscillations of vortex lattices in rotating Bose-Einstein condensates. *Phys. Rev. Lett.*, 92(6):060407, 2004.

[57] E. J. Mueller. Spin textures in slowly rotating Bose-Einstein condensates. *Phys. Rev. A*, 69(033606), 2004.

[58] E. J. Mueller and Tin-Lun Ho. Two-component Bose-Einstein condensates with a large number of vortices. *Phys. Rev. Lett.*, 88(18):180403, 2002.

[59] C. Orzel, A. K. Tuchman, M. L. Fenselau, M. Yasuda, and M. A. Kasevich. Squeezed states in a Bose-Einstein condensate. *Science*, 291(5512):2386, 2001.

[60] V. M. Pérez-García, Humberto Michinel, J. I. Cirac, M. Lewenstein, and P. Zoller. Dynamics of Bose-Einstein condensates: Variational solutions of the Gross-Pitaevskii equations. *Phys. Rev. A*, 56(2):1424, 1997.

[61] C. J. Pethick and H. Smith. *Bose-Einstein Condensation in Dilute Gases*. Cambridge Univ. Press, 1. edition, 2002.

[62] L. P. Pitaevskii. Vortex lines in an imperfect Bose gas. *Sov. Phys. JETP*, 13(2):451, 1961.

[63] P. A. Ruprecht, M. J. Holland, K. Burnett, and M. Edwards. Time-dependent solution of the nonlinear Schrödinger equation for Bose-condensed trapped neutral atoms. *Phys. Rev. A*, 51(6):4704, 1995.

[64] B. I. Schneider and D. L. Feder. Numerical approach to the ground and excited states of a Bose-Einstein condensed gas confined in a completely anisotropic trap. *Phys. Rev. A*, 59(3):2232, 1999.

[65] M. P. Singh and A. L. Satheesha. Ground state and vortex states of bosons in an anisotropic trap: A variational approach. *Euro. Phys. J. D*, 7(3):391–398, 1999.

[66] J. Sinova, C. B. Hanna, and A. H. MacDonald. Quantum melting and absence of Bose-Einstein condensation in two-dimensional vortex matter. *Phys. Rev. Lett.*, 89(3):030403, 2002.

[67] E. B. Sonin. Vortex oscillations and hydrodynamics of superfluids. *Rev. Mod. Phys*, 59(87), 1987.

[68] E. B. Sonin. Continuum theory of Tkachenko modes in rotating Bose-Einstein condensate. *Phys. Rev. A*, 71(1):011603, 2005.

[69] E. B. Sonin. Ground state and Tkachenko modes of a rapidly rotating Bose-Einstein condensate in the lowest-Landau-level state. *Phys. Rev. A*, 72(2):021606, 2005.

[70] V. K. Tkachenko. On vortex lattices. *JETP*, 22(6), 1966.

[71] V. K. Tkachenko. Stability of vortex lattices. *JETP*, 23(6), 1966.

[72] V. K. Tkachenko. Elasticity of vortex lattices. *JETP*, 29(5), 1969.

[73] P. Engels P. Mogendorff V. Schweikhard, I. Coddington and E. A. Cornell. Rapidly rotating Bose-Einstein Condensates in and near the Lowest Landau Level. *Phys. Rev. Lett.*, 93(210403), 2004.

[74] P. Engels S. Tung V. Schweikhard, I. Coddington and E. A. Cornell. Vortex lattice dynamics in rotating spinor Bose-Einstein Condensates. *Phys. Rev. Lett.*, 92(040404), 2004.

[75] A. D. B. Woods. *Quantum Fluids*. Number 242. North-Holland, Amsterdam, 1966.

[76] E. J. Yarmchuk and R. E. Packard. Photographic studies of quantized vortex lines. *Journal of Low Temperature Physics*, 46(5 - 6):479–515, 1982.

[77] H. Zhai, Q. Zhou, R. Lu, and L. Chang. Double-layer Bose-Einstein condensates with a large number of vortices. *Phys. Rev. A*, 69(6):063609, 2004.

[78] M. W. Zwierlein, J. R. Abo-Shaeer, A. Schirotzek, C. H. Schunck, and W. Ketterle. Vortices and superfluidity in a strongly interacting fermi gas. *Nature*, 435(7045):1047–1051, 2005.

Appendix A

Jacobi Theta Function

The general form of the wave function in the lowest Landau level is $\Psi(x,y) = f(z)e^{-r^2/2d^2}$, where $z = x + iy$ and f is an entire function whose zeros are accounted as vortices. We assume that these vortices form a regular lattice with basis vectors b_1 and $b_2 = b_1(u + iv)$, satisfying $\{b = n_1 b_1 + n_2 b_2\}$, where n_i are integers. Then the unit cell size is $v_c = b_1^2 v$. The Jacobi theta function $\theta(\zeta, \tau)$ is a quasiperiodic function with periodic zeros, where $\zeta = (x + iy)/b_1, \tau = u + iv$. It is given with an infinite summation as,

$$\theta(\zeta,\tau) = \frac{1}{i}\sum_{n=-\infty}^{\infty}(-1)^n e^{i\pi\tau(n+1/2)^2}e^{2\pi i\zeta(n+1/2)}. \tag{A.1}$$

The quasiperiodicity of the function comes from,

$$\theta(\zeta+1,\tau) = -\theta(\zeta,\tau), \tag{A.2}$$

$$\theta(\zeta+\tau,\tau) = -e^{-i\pi(\tau+2\zeta)}\theta(\zeta,\tau), \tag{A.3}$$

Then $f(z)$ can be written using JTF and an entire function without zeros in its general form. The only constraint is the normalizability of the wave function which restricts the form of entire function as $h(\zeta) = \exp(c_1\zeta + c_2\zeta^2)$. The density of the system is given by $|\Psi(\mathbf{r})|^2 = |\theta(\zeta,\tau)|^2|e^{c_1\zeta+c_2\zeta^2}|^2 e^{-r^2/d^2}$.

$$|\theta(\zeta,\tau)|^2 = \textstyle\sum_m (-1)^m e^{2\pi i m\bar{x}} e^{-\pi v m^2/2} L_m \tag{A.4}$$

$$L_m = \frac{1}{2}\sum_{m'}\left(1 - e^{i\pi(m+m')}\right)e^{(i\pi um - 2\pi\bar{y} - \pi v m'/2)m'} \tag{A.5}$$

Here the coefficient $(1-e^{i\pi(m+m')}$ in L_m arises because of change of variables. We applied the Poisson summation formula which is given as,

$$\sum_{n=-\infty}^{\infty} f(n) = \sum_{k=-\infty}^{\infty} = \sum_{k=-\infty}^{\infty}\int_{-\infty}^{\infty} dx f(x)e^{-2\pi ikx} \tag{A.6}$$

to L_m and obtain,

$$L_m = \sqrt{\frac{1}{2v_c}}\sum_k (-1)^{(m+1)k} e^{\left(-\pi(k+um+2i\bar{y})^2/2v\right)}. \tag{A.7}$$

We then find,

$$|\theta(\zeta,\tau)|^2 = \left[\frac{1}{v_c}\sum_{\mathbf{K}} g_{\mathbf{K}} e^{i\mathbf{K}\cdot\mathbf{r}}\right] e^{2\pi y^2/v_c} \tag{A.8}$$

where $\mathbf{r} = x\hat{x} + y\hat{y}$,$\mathbf{K} = m_1\mathbf{K}_1 + m_2\mathbf{K}_2$, and $\mathbf{K}_i$ are the basis vector of the reciprocal lattice, $\mathbf{K}_1 = (2\pi/v_c)\mathbf{B}_2 \times \hat{\mathbf{z}}$, $\mathbf{K}_2 = (2\pi/v_c)\hat{\mathbf{z}} \times \mathbf{B}_1$, and the Fourier coefficients are given as

$$g_{\mathbf{K}} = (-1)^{m_1+m_2+m_1m_2} e^{-v_c|\mathbf{K}|^2/8\pi}\sqrt{\frac{v_c}{2}}\ , \tag{A.9}$$

where

$$v_c\mathbf{K}^2 = \frac{(2\pi)^2}{v}\left((vm_1)^2 + (m_2 - um_1)^2\right). \tag{A.10}$$

From inversion symmetry about the origin $\mathbf{r} = 0$, we get $c_1 = 0$, and from the cylindrical symmetry, we have $c_2 = b_1^2\pi/(2v_c)$. The periodic function $g(\mathbf{r}) = g(\mathbf{r}+\mathbf{R})$ is given as,

$$g(\mathbf{r}) = |\theta\left(\zeta,\tau\right) exp(-\pi y^2/v_c)|^2. \tag{A.11}$$

In Ref. [40] it is shown that wave function in LLL can also be written as a gaussian with width σ multiplied by a periodic function $g(\mathbf{r})$. Then we see that $\sigma^{-2} = d^{-2} - \pi v_c^{-1}$.